# Mesozoic deep-water carbonate deposits from the southern Tethyan passive margin in Iran (Pichakun nappes, Neyriz area): biostratigraphy, facies sedimentology and sequence stratigraphy

Cécile Robin, Spela Gorican, François Guillocheau, Philippe Razin, Gilles Dromart and Hamid Mosaffa

*Geological Society, London, Special Publications* 2010; v. 330; p. 179-210
doi:10.1144/SP330.10

# Mesozoic deep-water carbonate deposits from the southern Tethyan passive margin in Iran (Pichakun nappes, Neyriz area): biostratigraphy, facies sedimentology and sequence stratigraphy

CÉCILE ROBIN[1]*, SPELA GORICAN[2], FRANÇOIS GUILLOCHEAU[1], PHILIPPE RAZIN[3], GILLES DROMART[4] & HAMID MOSAFFA[5]

[1]*Géosciences-Rennes, UMR 6118 Université de Rennes 1–CNRS, 35042 Rennes cedex, France*

[2]*Institute of Paleontology, ZRC SAZU, Gosposka 13, Sl-1000 Ljubljana, Slovenia*

[3]*EGID, Université de Bordeaux III, BP 06, 33401 Talence Cedex, France*

[4]*Laboratoire Sciences Terre, UMR 5570 Ecole Normale Supérieure de Lyon–Université de Lyon 1–CNRS, 69364 Lyon Cedex, France*

[5]*Geological Survey of Iran, PO Box 13185-1494, Tehran, Iran*

**Corresponding author (e-mail: cecile.robin@univ-rennes1.fr)*

**Abstract:** The objective of this work is to study the Mesozoic turbiditic sediments from the southern Tethys margin in Iran. These sediments are exposed as nappes in the Pichakun Mountains (i.e. the Zagros Mountains in the Neyriz area), which inverted during latest Cretaceous time. Radiolarians are used to both define and date four main lithostratigraphic formations: (1) the Bar Er Formation (undated, probably Late Triassic to Early Jurassic); (2) the Darreh Juve Formation (Aalenian–early Bajocian to middle Callovian–early Oxfordian); (3) the Imamzadeh Formation (middle Callovian–early Oxfordian to Aptian); (4) the Neghareh Khaneh Formation (late Aptian to Turonian–Coniacian). Most of the sediments are deep-sea gravity-flow lobe deposits. Channel deposits occurred during the Bajocian (i.e. the Darreh Juve Fm) and deeply incised channels (canyons?) occurred during the Albian (i.e. the Neghareh Khaneh Fm). Twenty-seven facies, grouped into eight facies associations, are defined. Based on a sequence stratigraphic study (i.e. the stacking pattern), five second-order cycles (10–30 Ma duration), defined between two successive distal facies time-intervals, are characterized: (1) the J2 (Toarcian?–middle Oxfordian, unconformity: Late Toarcian–Aalenian); (2) the J3 (middle Oxfordian–Berriasian, unconformity: middle? Tithonian); (3) the K1.1 (Berriasian–undated top); (4) the K1.2 (undated base–early Aptian, unconformity: late Hauterivian); (5) the K1.3 (early Aptian–at least Turonian–Coniacian, unconformity: Aptian–Albian boundary). The most important tectonic event recorded occurred at the Aptian–Albian boundary (a deposition of olistoliths, from a few metres to 100 m thick, in debris flows; related to Austrian deformations). The Arabian-scale late Toarcian and early Tithonian deformations have been recorded as unconformities. It is expected that another tectonic event occurred during the late Hauterivian. The unconformity of cycle K1.1 could be a late Valanginian eustatic fall of climatic origin.

During Jurassic and Cretaceous times, the Tethyan southern margin was a broad carbonate platform, stretching from Oman to Tunisia (Dercourt *et al.* 2000; Philip 2003). Because of their economic interest, these carbonate platform sediments have been extensively studied and several sequence stratigraphic and palaeogeographical publications are available (Murris 1980; Le Nindre *et al.* 1990; Grabowski & Norton 1994; Al-Husseini 1997; Sharland *et al.* 2001; Ziegler 2001; Haq & Al-Qahtani 2005). Conversely, only a limited number of available studies are dedicated to the deep-sea and the outer parts of the margin. These studies are mainly concerned with the nappes of deep-sea sediments of the Oman Mountains (Bernouilli & Weissert 1987; Béchennec *et al.* 1990; Le Métour *et al.* 1995; Pillevuit *et al.* 1997; Blechschmidt *et al.* 2004). Furthermore, most of these studies deal with palaeogeographical reconstructions, with an emphasis on the location, on a shelf–abyssal plain profile, of shallow isolated carbonate platforms (interpreted as seamount caps) and their relationships with different turbiditic systems.

A similar pattern seems to have developed along the southern Tethyan margin in Iran, with the occurrence of the Kermanshah and Neyriz exotic deposits (Ricou 1976; Hallam 1976; Braud 1989). Unfortunately, no sedimentological or

*From*: LETURMY, P. & ROBIN, C. (eds) *Tectonic and Stratigraphic Evolution of Zagros and Makran during the Mesozoic–Cenozoic*. Geological Society, London, Special Publications, **330**, 179–210.
DOI: 10.1144/SP330.10 0305-8719/10/$15.00 

sequence stratigraphic studies have been performed on these carbonate platforms or the associated turbiditic facies.

This study focuses on the turbiditic facies of the Iranian palaeomargin in the Neyriz area (i.e. the Zagros Mountains). The primary objective of the present study is to use radiolarians to date deep-water sediments from the Iranian Mesozoic Tethyan southern margin and to characterize their depositional environments, the associated stratigraphic cycles, and their tectonic or eustatic causes.

## Geological setting

The studied outcrops are located SW of Neyriz (Fig. 1), in the Zagros Mountains along the 'Crush' Zone (i.e. the Zagros Thrust Zone or High Zagros Belt; Stocklin 1968; Berberian & King 1981; Alavi 1994), which is the suture of the Tethys Ocean closure. All of the sediments from the outer margin and the oceanic crust crop out as nappes, which have been thrust over the autochthonous shallow carbonate deposits of the Arabian platform. Four tectonic units were defined in the study area (Ricou 1976; Hallam 1976): (1) the autochthonous Arabian platform (Sarvak Fm, Cenomanian–Turonian); (2) the Pichakun nappes (Pichakun Series, Late Triassic to Cenomanian); (3) the 'Mélange' or Bakhtegan Beds of Hallam (1976), with carbonate blocks of Late Triassic age (Ricou 1976); (4) the ophiolite suite (Neyriz Ophiolites). The three former formations are stacked, thrust units, which are unconformably overlain by shallow-water reefal limestones of Maastrichtian age (James & Wynd 1965). These latest Cretaceous shallow-water sediments were thrust during the Pliocene (Ricou 1976) by the Sanadaj–Sirjan metamorphic units along the Main Zagros Thrust. A margin inversion took place during the Late Cretaceous, between the Cenomanian (the youngest sediments of the Pichakun nappes) and the Maastrichtian (unconformably overlapping sediments).

The 'Mélange' or Bakhtegan Beds and equivalent rocks along the Arabian platform (i.e. the Bisitoun or Bisotun Limestones in the Kermanshah area (Braud 1989), and the Kawr Group in Oman (Bernouilli & Weissert 1987; Pillevuit *et al.* 1997), are interpreted as deposits on an isolated carbonate platform located on top of a seamount (Searle & Graham 1982; Stampfli *et al.* 1991; Dercourt *et al.* 2000). The Pichakun unit is made up of turbiditic deposits ('flysch') located between the Arabian carbonate platform and the isolated carbonate platform (or possible seamount) named the 'Mélange' by Ricou (1976) (i.e. the Neyriz Seamount). The nature of the crust below these turbiditic sediments and the significance of these isolated carbonate platforms are a matter of discussion: is the crust oceanic (Searle & Graham 1982) or thinned continental (Braud 1989; Lapierre *et al.* 2004)? Do carbonates represent real top seamount sediments (Searle & Graham 1982) or deposits of subsiding tilted blocks (Braud 1989)?

The Pichakun nappes are exposed in the Pichakun Mountains, between Lake Bakhtegan and Lake Tashk (Fig. 1b), and consist of a stack of at least 10 southward thrust units (Ricou 1976). Because of refolding of the stacked nappes, the geometrical relationship of the thrust units between the southern and northern sides of these nappes remains unclear (Ricou 1976).

## Methods

Since the studies by Hallam (1976) and Ricou (1976), no study has applied the modern principles of sedimentology and stratigraphy to deep-sea marine sediments from the southern Tethyan margin in Iran.

The Pichakun nappes (Fig. 1b), which are composed of different types of gravity-flow deposits, do not represent the whole margin. Most of the tectonic units either have been eroded or do not crop out. Thus, this study does not aim to reconstruct the complete geometry of the margin. Only correlations between measured sections, based on biostratigraphic data (radiolarians) and the stacking pattern (sequence stratigraphy) of the gravity-flow deposits, were carried out.

Three main tectonic units (Ricou 1976) were studied (Fig. 1b): the Imamzadeh unit (three measured sections); the Darreh Juve unit (one measured section); the Bar Er unit (one measured section).

### *Lithostratigraphy and biostratigraphy*

The definition of the lithostratigraphic units is based on the recommendations of the International Stratigraphy Guide of the International Commission of Stratigraphy (ICS; http://www.stratigraphy.org).

The biostratigraphy is based on the study of radiolarians in cherts and siliceous limestones. Siliceous limestones were processed with acetic acid (10%) and then with hydrofluoric (5%) acid, whereas the chert samples were processed with hydrofluoric acid only. Dating is primarily based on the following zonations: Baumgartner *et al.* (1995) for the Middle and Late Jurassic; Jud (1994) for the late Tithonian to Barremian; O'Dogherty (1994) for the Aptian to Turonian interval.

### *Facies sedimentology*

Several sedimentary facies (lithology, sedimentary structures, rare trace fossils) were defined and

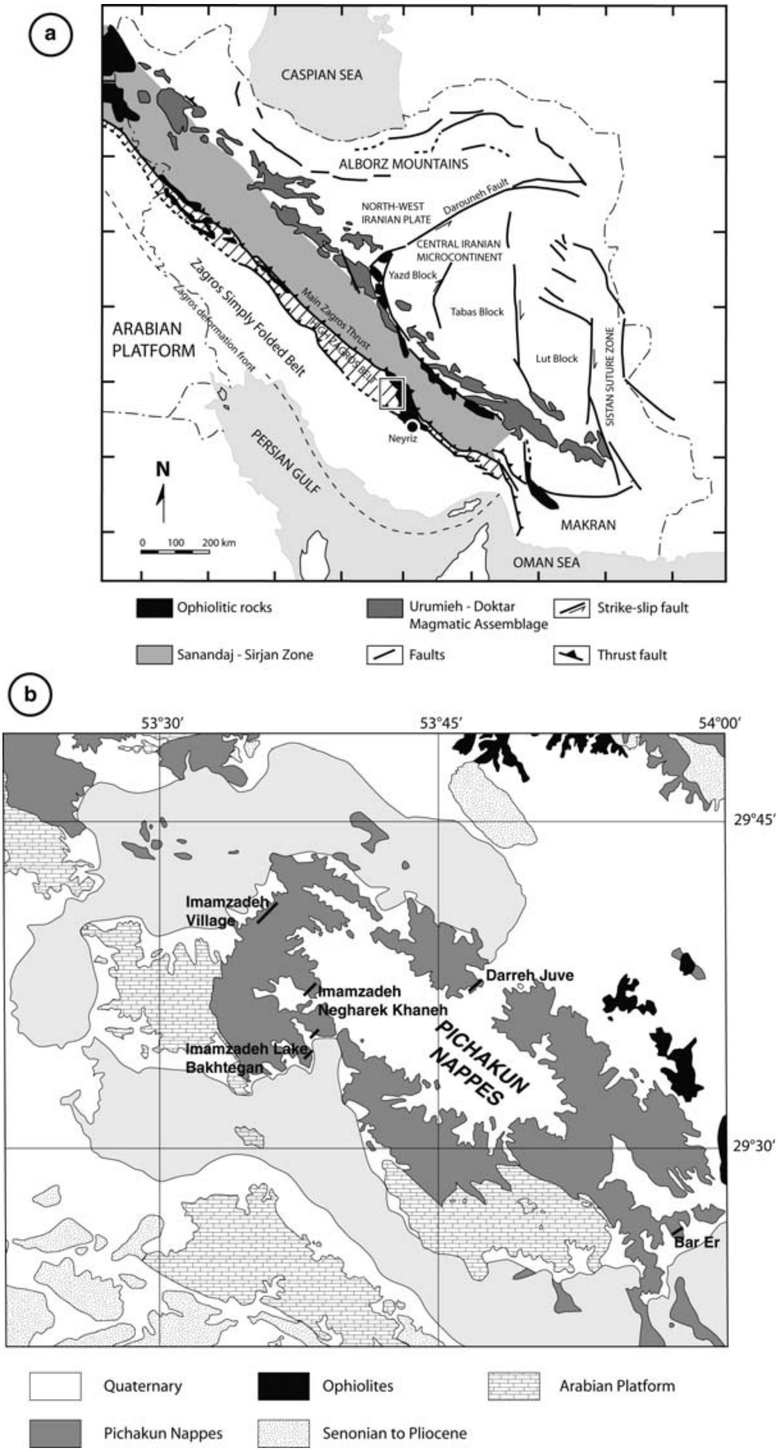


**Fig. 1.** Location map of the study area. (**a**) Structural map of Iran (modified from Stocklin 1968). (**b**) Simplified geological map of the Pichakun Nappes and location of the sections (from the National Iranian Oil Company, geological map of Shiraz at 1:250 000, Tehran 1979, 2nd ed.).

grouped into facies associations. Facies associations are more characteristic of depositional environments, rather than, as in the case of deep-sea gravity-flow deposits, facies that record both elementary hydrodynamic processes and the nature of upstream sediment sources. A palaeocurrent study was performed to determine the location of the source areas and the hydrodynamic processes. All of the studied sections are now preserved as thrust units. Palaeomagnetic analyses to quantify possible tectonic rotations occurring at the time of nappe emplacements were not carried out on these outcrops. This implies that palaeocurrent data must be used with caution.

### *Sequence stratigraphy: correlations*

The application of sequence stratigraphy, and mainly the stacking pattern technique (i.e. the correlation of wells or outcropping sections, Van Wagoner *et al.* 1988, 1990; Homewood *et al.* 1999), to deep-sea gravity-flow deposits has been mainly carried out in siliciclastic systems (e.g. Mutti 1985; Posamentier *et al.* 1988). The interpretation of stratigraphic sequences in carbonate gravity-flow deposits is more complex than for terrigenous sediments (Eberli 1991). Carbonate production on the shelf and thus the nature and volume of sediments available for resedimentation along the slope are highly dependent on the response of the carbonate factory to relative sea-level fluctuations (Eberli 1991; Handford & Loucks 1993; Pomar 2001). No suitable predictive models are available, in contrast to those that are refined for siliciclastic gravity-flow deposits (e.g. Mutti 1985; Mutti *et al.* 1999; Posamentier *et al.* 1988). Since the publication of the classical works by Eberli (1991) and Schlager *et al.* (1994), most researchers agree that carbonate turbiditic deposition occurs during high relative sea level (i.e. highstand shedding) and that almost no deposition occurs during low relative sea level (i.e. emersion and no carbonate sediment production). In contrast, most of the siliciclastic turbidite deposits occur at the time of the maximum rate of relative sea-level fall (Posamentier *et al.* 1988).

The 'stacking pattern' technique is based on the migration of the depositional profile along a proximal (landward) to distal (seaward) trend (Van Wagoner *et al.* 1988, 1990; Homewood *et al.* 1999). This implies the building of an 'ideal' depositional profile that will be the basis for defining the distal-up and proximal-up trends throughout the different sections. However, this general facies model remains an approximation of the real conditions. First, facies may change laterally along the depositional profile; not only along the channels but also on the lobes. The lateral substitution of some facies needs to be taken into account. Second, depositional profiles may change according to the volume and the grain size of the sediments. At a time of low carbonate supply from the platform, condensation or radiolarite deposition has to be expected and the use of the complete depositional model becomes meaningless. Probably, most of the distal–proximal cycles defined in this paper do not record migrations of the same profile, but rather a change in the carbonate supply from the platform.

The relationship between the three depositional sequence surface types on the platform (i.e. unconformity, flooding or transgressive surface and maximum flooding surface) for sedimentary cycles in deep-sea environments is subject to discussion (e.g. Posamentier *et al.* 1988; Mutti *et al.* 1999). The unconformity surface is the only one that is fully accepted by all researchers. It is interpreted as recording a sharp facies change from distal to proximal facies (i.e. a downward shift of facies). In this paper, the most distal facies time interval of a cycle is the equivalent of the maximum flooding surface on the platform. For the most proximal facies time period of the cycle, we have defined what is here named the proximal turn-around surface. This surface either may coincide with the unconformity or may occur later. An *a priori* relationship with the flooding surface on the shelf is not expected.

## Lithostratigraphy

Four main lithostratigraphic units, corresponding to the four lithological units recognized by Ricou (1976), are presented in Figure 2. They are mappable units that range from several tens of metres to a few hundreds of metres thick and that correspond to lithostratigraphic formations. All of these new formations (Fm) are named from type-section localities in the Neyriz area; they are, from base to top, the Bar Er Fm, the Darreh Juve Fm, the Imamzadeh Fm and the Neghareh-Khaneh Fm (Fig. 2).

### *The Bar Er Formation*

The Bar Er Fm corresponds to the black marls ('Marnes noires') previously described by Ricou (1976). This formation was defined near the village of Bar Er (29°26.254′N, 53°55.584′E). It is mainly composed of black shales, more or less calcareous, alternating with thick conglomerates (1–25 m). Most of the conglomerates are matrix-supported (clays to silts) with reef clasts a few centimetres to metres in size. Some bioclastic limestones, a few decimetres thick, are interbedded within these alternations. The conglomeratic beds range from a

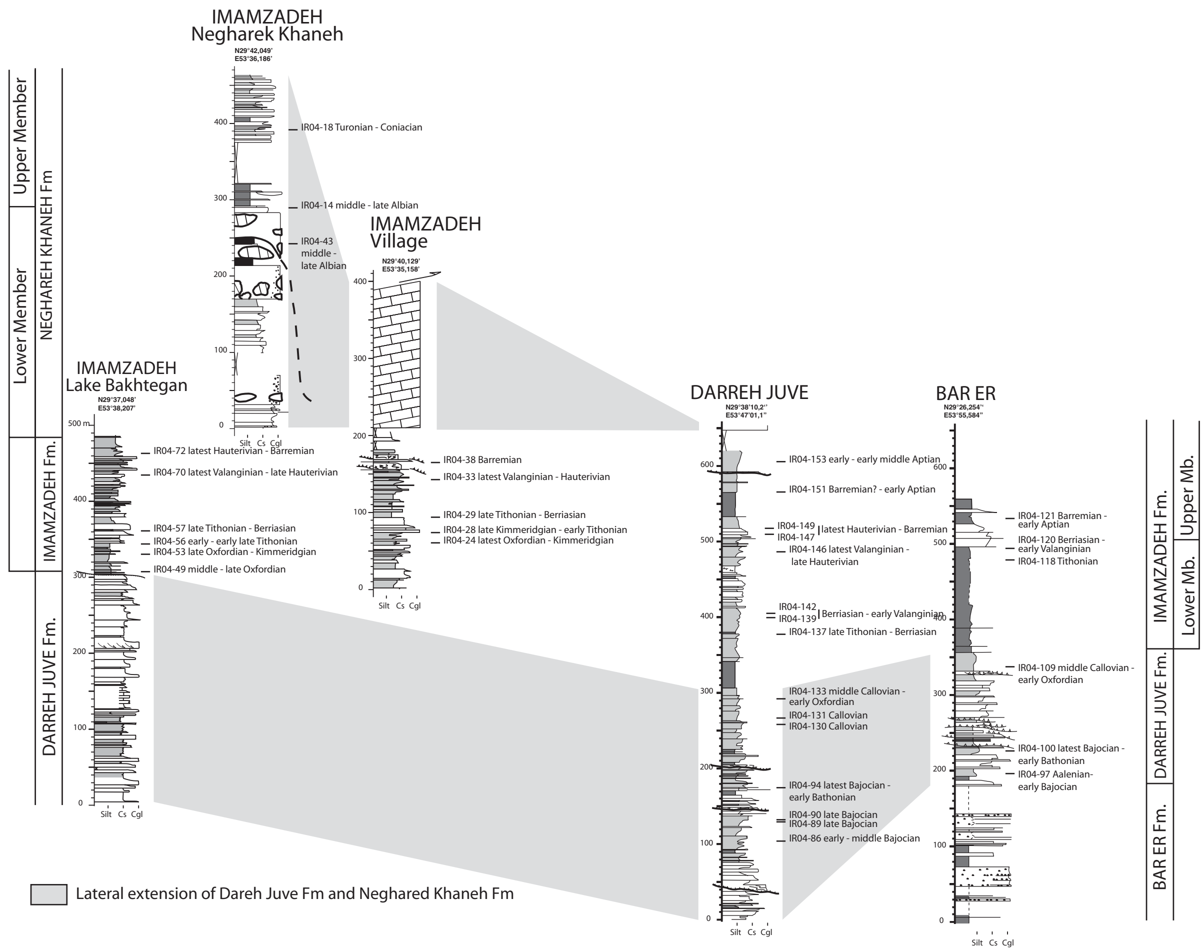


**Fig. 2.** Lithostratigraphy and biostratigraphy of the five studied sections from the Pichakun area.

few metres to 15 m thick. The base of this formation is always thrust. Its minimum thickness is about 180 m in the Bar Er type-section.

As suggested by Ricou (1976), the large clasts from the reef are resedimented from the carbonate platforms. The reworked foraminifers (M. Lys, cited by Ricou 1976) indicate a minimum Late Triassic age. Therefore, this formation could be Late Triassic to Early Jurassic in age.

### *The Darreh Juve Formation*

The Darreh Juve Formation corresponds to the siliceous limestones ('Calcaires siliceux') described by Ricou (1976). The type-section of this formation is located near the village of Darreh Juve (29°38′10.2″N, 53°47′01.1″E). It is mainly composed of massive limestone rock units (the grain sizes range from sands to conglomerates) with some heterolithic levels (i.e. alternations of siliciclastic claystones or muddy limestones with sand-grained clastic limestones). The thickness of this formation (170 m) can be estimated in the Bar Er section, the only place where the boundary with the underlying formation was observed (Fig. 2). A thickness of 300 m has been preserved (because of the thrust nature of the lower boundary in this unit) in the type-section and in the Imamzadeh–Lake Bakhtegan section. The top of the Darreh Juve Formation could be either sharp, with an erosional surface (i.e. the Imamzadeh–Lake Bakhtegan section) or progressive, with a decrease in the bed thickness. This formation passes upward into the green and/or reddish cherts and shales of the Imamzadeh Formation.

The lithology of this unit changes throughout the various thrust units, from more massive homolithic coarse-grained limestones with matrix-supported conglomerates (i.e. the Imamzadeh–Lake Bakhtegan section) to more heterolithic fine-grained limestones (i.e. the Bar Er section). The massive homolithic facies of this unit are dominated by ooid packstones to grainstones, with some echinoid fragments, or other bioclasts, in a micritic matrix. These coarse-grained limestones alternate with heterolithic levels composed of green and reddish shales and silicified limestones. The ratio between the homolithic and heterolithic levels varies laterally. The more heterolithic facies are dominated by shaly and silicified fine-grained limestone alternations.

### *The Imamzadeh Formation*

The Imanzadeh Fm corresponds to the radiolarites described by Ricou (1976). The type-section of this formation is located along two sections in the Imamzadeh area: near Lake Bakhtegan (29°37.048′N, 53°38.207′E, the base of the formation) and near the village (29°40.129′N, 53°35.158′E, the top of the formation). It is mainly composed of an alternation of shales to true cherts with silicified limestones. Some coarser-grained bioclastic levels (medium- to coarse-grained sands with rare conglomerates) can occur. The thickness of this formation (which is composed of two members) was estimated to be about 240 m in the Darreh Juve section, the only place where the base and top boundaries are observed (Fig. 2).

The lower member is exposed in the southern part of the Bar Er village. The type-section crops out along the valley, between two hills (29°26.254′N, 53°55.584′E). It is primarily composed of red to green shales, cherts (radiolarites) and silicified limestones (an alternation of muddy limestones and fine sand-grained bioclastic limestones). Its thickness varies from 40 m (the Imamzadeh–Lake Bakhtegan section) to 140 m (the Bar Er section). The lithology of this member changes throughout the various thrust units, from more heterolithic (the Imamzadeh–Lake Bakhtegan section) to more homolithic shaly facies (the Bar Er section).

The upper member has been defined near Lake Bakhtegan, on the northern border of the Bakhtegan Lake and north of the Kuhe Na Anhir hills (29°37.048′N, 53°38.207′E). This member records a more or less sharp transition from the underlying member and is made of an alternation of fine-grained (almost completely silicified) limestones with locally silicified medium- to very coarse sand-grained bioclastic limestones (10 cm to 1 m thick) with some clast-supported conglomerates. The characteristic of this upper member, compared with the lower member, is the lack of shales and primary cherts. Generally, the top contact of this member is thrust.

### *The Neghareh-Khaneh Formation*

The Neghareh-Khaneh Fm corresponds to the conglomeratic limestones ('Calcaires conglomératiques') described by Ricou (1976). The type-section of this formation is located on the outcrops overhanging the sanctuary of Imazadeh, near the hamlet of Neghareh-Khaneh (29°42.049′N, 53°36.186′E). It is made up of massive conglomerates interbedded with alternations of shales and limestones that are a few decimetres thick. The upper part of the formation is composed only of shale and limestone alternations. The base of this formation is sharp and erosional, whereas its top is always thrust. In the type-section, the formation, which is composed of two members, is 450 m thick.

The lower member is made up of thick conglomerates (5–250 m) infilling palaeocanyons with very large blocks (10–200 m). These blocks (true olistoliths) are composed of various types of carbonate platform deposits (mainly inner shelf: mud, stromatolites, oncoids, etc.). Either sand-grained bioclastic limestones or alternations of claystones and cherts may be interbedded with these conglomerates.

The upper member is an alternation of claystones, cherts and clastic limestones. Their grain sizes range from fine-grained limy sands to conglomerates.

## Biostratigraphy

Radiolarians were analysed from samples of radiolarian cherts and siliceous limestones from the Darreh Juve, Imamzadeh and Neghareh Khaneh Formations. The preservation of radiolarians ranges from poor to moderate. A list of stratigraphically important species is given in Table 1. Sample locations are shown in Figure 2. The characteristic species are illustrated in Figures 3–5.

The oldest radiolarians are Aalenian to Bajocian in age (Fig. 3 and Table 1) and were found in the lower part of the Darreh Juve Formation in an interval several tens of metres thick, composed almost entirely of cherts with only rare resedimented-limestone beds. In sample IR04-89 from Darreh Juve, the co-occurrence of *Williriedellum marcucciae* Cortese (FAD in UA Zone 4 of Baumgartner *et al.* 1995) with *Hexasaturnalis suboblongus* (Yao) (the entire range in the Bajocian; see

**Table 1.** *Radiolarian inventory and age of samples*

| Sample | Radiolarians | Age |
|---|---|---|
| *Darreh Juve section* | | |
| IR04-86 | *Acaeniotylopsis variatus* (Ozvoldova)<br>*Hsuum* cf. *matsuokai* Isozaki & Matsuda<br>*Thurstonia* sp.<br>*Trillus* sp.<br>*Tympaneides* sp.<br>*Unuma* cf. *typicus* Ichikawa & Yao | Early–middle Bajocian |
| IR04-89 | *Dictyomitrella*? *kamoensis* Mizutani & Kido<br>*Hexasaturnalis suboblongus* (Yao)<br>*Protunuma fusiformis* Ichikawa & Yao<br>*Stichomitra*? *takanoensis* Aita<br>*Tethysetta dhimenaensis* (Baumgartner)<br>*Williriedellum marcucciae* Cortese | Late Bajocian |
| IR04-90 | *Dictyomitrella*? *kamoensis* Mizutani & Kido<br>*Stichomitra*? *takanoensis* Aita<br>*Striatojaponocapsa plicarum* (Yao)<br>*Unuma darnoensis* Kozur | Late Bajocian |
| IR04-94 | *Williriedellum tetragonum* (Matsuoka)<br>*Williriedellum yaoi* (Kozur) | Latest Bajocian–early Bathonian |
| IR04-130 | *Eucyrtidiellum nodosum* Wakita<br>*Eucyrtidiellum ptyctum* (Riedel & Sanfilippo)<br>*Dictyomitrella*? *kamoensis* Mizutani & Kido<br>*Plicaforacapsa catenarum* (Matsuoka)<br>*Praewilliriedellum robustum* (Matsuoka)<br>*Pseudoeucyrtis firma* Hull<br>*Pseudoristola tsunoensis* (Aita)<br>*Striatojaponocapsa conexa* (Matsuoka)<br>*Williriedellum yaoi* (Kozur) | Callovian |
| IR04-131 | *Higumastra imbricata* (Ozvoldova)<br>*Guexella nudata* (Kocher)<br>*Pseudoeucyrtis firma* Hull<br>*Ristola procera* (Pessagno)<br>*Striatojaponocapsa conexa* (Matsuoka) | Callovian |
| IR04-133 | *Angulobracchia purisimaensis* (Pessagno)<br>*Cinguloturris carpatica* Dumitrica<br>*Eucyrtidiellum nodosum* Wakita<br>*Mirifisus guadalupensis* Pessagno | Middle Callovian–early Oxfordian |

(*Continued*)

**Table 1.** *Continued*

| Sample | Radiolarians | Age |
|---|---|---|
| | *Protunuma japonicus* Matsuoka & Yao | |
| | *Tritrabs casmaliaensis* (Pessagno) | |
| | *Williriedellum carpathicum* Dumitrica | |
| IR04-137 | *Angulobracchia portmanni* Baumgartner | Late Tithonian–Berriasian |
| | *Cinguloturris cylindra* Kemkin & Rudenko | |
| | *Dicerosaturnalis dicranacanthos* (Squinabol) | |
| | *Emiluvia chica* (Foreman) | |
| | *Hsuum mclaughlini* Pessagno & Blome | |
| | *Neorelumbra buwaydahensis* Kiessling | |
| | *Pseudodictyomitra carpatica* (Lozyniak) | |
| | *Tethysetta boesii* (Parona) | |
| IR04-139 | *Angulobracchia portmanni* Baumgartner | Berriasian–early Valanginian |
| | *Cinguloturris cylindra* Kemkin & Rudenko | |
| | *Dicerosaturnalis dicranacanthos* (Squinabol) | |
| | *Emiluvia chica* (Foreman) | |
| | *Hiscocapsa kaminogoensis* (Aita) | |
| | *Hsuum* sp. | |
| | *Neorelumbra buwaydahensis* Kiessling | |
| | *Pantanellium squinaboli* (Tan) | |
| | *Pseudodictyomitra carpatica* (Lozyniak) | |
| | *Tethysetta boesii* (Parona) | |
| IR04-142 | *Angulobracchia portmanni* Baumgartner | Berriasian–early Valanginian |
| | *Dicerosaturnalis dicranacanthos* (Squinabol) | |
| | *Emiluvia chica* (Foreman) | |
| | *Hiscocapsa kaminogoensis* (Aita) | |
| | *Hsuum* sp. | |
| | *Neorelumbra buwaydahensis* Kiessling | |
| | *Pantanellium squinaboli* (Tan) | |
| | *Tethysetta boesii* (Parona) | |
| IR04-146 | *Aurisaturnalis variabilis* (Squinabol) | Latest Valanginian–late Hauterivian |
| | *Cecrops septemporatus* (Parona) | |
| | *Crolanium* sp. | |
| | *Crucella*? *inflexa* (Rüst) | |
| | *Dicerosaturnalis dicranacanthos* (Squinabol) | |
| | *Dicerosaturnalis trizonalis* (Rüst) | |
| | *Hemicryptocapsa capita* (Tan) | |
| | *Tethysetta usotanensis* (Tumanda) | |
| IR04-147 | *Aurisaturnalis carinatus* (Foreman) | Latest Hauterivian–Barremian |
| | *Cryptamphorella conara* (Foreman) | |
| | *Dactyliodiscus lenticulatus* (Jud) | |
| | *Dictyomitra pseudoscalaris* Tan | |
| | *Hiscocapsa uterculus* (Parona) | |
| | *Tethysetta boesii* (Parona) | |
| IR04-149 | *Archaeodictyomitra lacrimula* (Foreman) | Latest Hauterivian–Barremian |
| | *Dibolachras tytthopora* Foreman | |
| | *Hiscocapsa uterculus* (Parona) | |
| | *Pseudodictyomitra lanceloti* Schaaf | |
| | *Suna hybum* (Foreman) | |
| | *Tethysetta boesii* (Parona) | |
| | *Tethysetta usotanensis* (Tumanda) | |
| | *Thanarla pacifica* Nakaseko & Nishimura | |
| IR04-151 | *Archaeodictyomitra lacrimula* (Foreman) | Barremian?–early Aptian |
| | *Aurisaturnalis carinatus perforatus* Dumitrica & Dumitrica-Jud | |
| | *Dictyomitra pseudoscalaris* Tan | |
| | *Mictyoditra pseudodecora* (Tan) | |
| | *Pantanellium* spp. | |
| | *Pseudodictyomitra* cf. *carpatica* (Lozyniak) | |
| | *Pseudodictyomitra lanceloti* Schaaf | |

(*Continued*)

**Table 1.** *Continued*

| Sample | Radiolarians | Age |
|---|---|---|
| | *Suna hybum* (Foreman) | |
| | *Tethysetta boesii* (Parona) | |
| | *Tethysetta usotanensis* (Tumanda) | |
| | *Thanarla pacifica* Nakaseko & Nishimura | |
| IR04-153 | *Archaeodictyomitra lacrimula* (Foreman) | Early–early middle Aptian |
| | *Dactyliodiscus lenticulatus* (Jud) | |
| | *Pseudodocrolanium puga* (Schaaf) | |
| *Barer Section* | | |
| IR04-97 | *Elodium pessagnoi* Yeh & Cheng | Aalenian–?early Bajocian |
| | *Hsuum altile* Hori & Otsuka | |
| | *Hsuum exiguum* Yeh & Cheng | |
| | *Parahsuum*? *natorense* (El Kadiri) | |
| | *Praeparvicingula nanoconica* (Hori & Otsuka) | |
| | *Trillus* sp. | |
| IR03-03 | *Stichomitra*? *takanoensis* Aita | Latest Bajocian–early Bathonian |
| | *Williriedellum marcucciae* Cortese | |
| | *Williriedellum tetragonum* (Matsuoka) | |
| IR04-109 | *Cinguloturris carpatica* Dumitrica | Middle Callovian–early Oxfordian |
| | *Emiluvia premyogii* Baumgartner | |
| | *Eucyrtidiellum ptyctum* Riedel & Sanfilippo | |
| | *Protunuma japonicus* Matsuoka & Yao | |
| | *Spongocapsula palmerae* Pessagno | |
| | *Transhsuum brevicostatum* (Ozvoldova) | |
| | *Tritrabs casmaliaensis* (Pessagno) | |
| IR04-118 | *Archaeodictyomitra apiarium* (Rüst) | Tithonian |
| | *Dicerosaturnalis dicranacanthos* (Squinabol) | |
| | *Emiluvia chica* Foreman | |
| | *Eucyrtidiellum pyramis* (Aita) | |
| | *Mirifisus dianae minor* (Baumgartner) | |
| | *Paronaella*? *tubulata* Steiger | |
| | *Podocapsa amphitreptera* Foreman | |
| | *Protunuma japonicus* Matsuoka & Yao | |
| | *Syringocapsa longituba* Steiger & Steiger | |
| IR04-120 | *Archaeodictyomitra apiarium* (Rüst) | Berriasian–early Valanginian |
| | *Cinguloturris cylindra* Kemkin & Rudenko | |
| | *Dicerosaturnalis dicranacanthos* (Squinabol) | |
| | *Fultacapsa tricornis* (Jud) | |
| | *Mirifisus dianae minor* (Baumgartner) | |
| | *Obesacapsula polyedra* (Steiger) | |
| | *Pseudodictyomitra carpatica* (Lozyniak) | |
| | *Pantanellium squinaboli* (Tan) | |
| | *Ristola cretacea* (Baumgartner) | |
| | *Tethysetta boesii* (Parona) | |
| IR04-121 | *Aurisaturnalis carinatus perforatus* Dumitrica & Dumitrica-Jud | Barremian–early Aptian |
| | *Archaeodictyomitra lacrimula* (Foreman) | |
| | *Cryptamphorella conara* (Foreman) | |
| | *Dicerosaturnalis trizonalis* (Rüst) | |
| | *Podobursa* sp. | |
| | *Tethysetta usotanensis* (Tumanda) | |
| *Imamzadeh–Lake Bakhtegan section* | | |
| IR04-49 | *Acastea diaphorogona* (Foreman) | Middle–late Oxfordian |
| | *Cinguloturris carpatica* Dumitrica | |
| | *Emiluvia ordinaria* Ozvoldova | |
| | *Emiluvia orea* Baumgartner | |
| | *Protunuma japonicus* Matsuoka & Yao | |

(*Continued*)

**Table 1.** *Continued*

| Sample | Radiolarians | Age |
|---|---|---|
| | *Sethocapsa* aff. *horokanaiensis* Kawabata | |
| | *Tethysetta mashitaensis* (Mizutani) | |
| | *Transhsuum brevicostatum* (Ozvoldova) | |
| | *Williriedellum crystallinum* Dumitrica | |
| | *Zhamoidellum ovum* Dumitrica | |
| IR04-53 | *Cinguloturris carpatica* Dumitrica | Latest Oxfordian–Kimmeridgian |
| | *Mirifusus dianae* (Karrer) | |
| | *Orbiculiforma*? *lowreyensis* Pessagno | |
| | *Parahsuum* sp. | |
| | *Paronaella cava* (Ozvoldova) | |
| | *Podocapsa amphitreptera* Foreman | |
| | *Protunuma japonicus* Matsuoka & Yao | |
| | *Pseudoeucyrtis reticularis* Matsuoka & Yao | |
| | *Ristola altissima altissima* (Rüst) | |
| | *Spongocapsula perampla* (Rüst) | |
| | *Syringocapsa longituba* Steiger & Steiger | |
| | *Tethysetta mashitaensis* (Mizutani) | |
| | *Williriedellum crystallinum* Dumitrica | |
| | *Zhamoidellum ovum* Dumitrica | |
| IR04-56 | *Archaeodictyomitra apiarium* (Rüst) | Early–early late Tithonian |
| | *Cinguloturris fusiforma* Hori | |
| | *Cinguloturris cylindra* Kemkin & Rudenko | |
| | *Dicerosaturnalis trizonalis* (Rüst) | |
| | *Eucyrtidiellum pyramis* (Aita) | |
| | *Mirifusus dianae* (Karrer) | |
| | *Podocapsa amphitreptera* Foreman | |
| | *Protunuma japonicus* Matsuoka & Yao | |
| | *Pseudodictyomitra carpatica* (Lozyniak) | |
| | *Ristola cretacea* (Baumgartner) | |
| | *Sethocapsa horokanaiensis* Kawabata | |
| | *Syringocapsa longituba* Steiger & Steiger | |
| IR04-57 | *Cinguloturris cylindra* Kemkin & Rudenko | Late Tithonian–Berriasian |
| | *Deviatus diamphidius* (Foreman) | |
| | *Dicerosaturnalis dicranacanthos* (Squinabol) | |
| | *Emiluvia chica* (Foreman) | |
| | *Emiluvia hopsoni* Pessagno | |
| | *Eucyrtidiellum pyramis* (Aita) | |
| | *Hiscocapsa kaminogoensis* (Aita) | |
| | *Hsuum raricostatum* Jud | |
| | *Mirifisus dianae minor* (Baumgartner) | |
| | *Neorelumbra tippitae* Kiessling | |
| | *Pantanellium squinaboli* (Tan) | |
| | *Paronaella*? *tubulata* Steiger | |
| | *Praeparvicingula cosmoconica* (Foreman) | |
| | *Pseudodictyomitra carpatica* (Lozyniak) | |
| | *Fultacapsa tricornis* (Jud) | |
| | *Svinitzium depressum* (Baumgartner) | |
| | *Tethysetta boesii* (Parona) | |
| | *Tricolocapsa*? *campana* Kiessling | |
| | *Williriedellum* aff. *crystallinum* Dumitrica | |
| IR04-70 | *Acaeniotyle umbilicata* (Rüst) | Latest Valanginian–late Hauterivian |
| | *Aurisaturnalis variabilis variabilis* (Squinabol) | |
| | *Cecrops septemporatus* (Parona) | |
| | *Crolanium bipodium* (Parona) | |
| | *Crucella bossoensis* Jud | |
| | *Dicerosaturnalis dicranacanthos* (Squinabol) | |
| | *Dictyomitra pseudoscalaris* Tan | |
| | *Hemicryptocapsa capita* (Tan) | |

(*Continued*)

**Table 1.** *Continued*

| Sample | Radiolarians | Age |
|---|---|---|
| | *Hiscocapsa kaminogoensis* (Aita) | |
| | *Suna hybum* (Foreman) | |
| | *Syringocapsa limatum* Foreman | |
| | *Tethysetta usotanensis* (Tumanda) | |
| IR04-72 | *Archaeodictyomitra lacrimula* (Foreman) | Latest Hauterivian–Barremian |
| | *Crolanium* sp. | |
| | *Dibolachras tytthopora* Foreman | |
| | *Dicerosaturnalis dicranacanthos* (Squinabol) | |
| | *Dicerosaturnalis trizonalis* (Rüst) | |
| | *Hiscocapsa uterculus* (Parona) | |
| | *Pantanellium* sp. | |
| | *Pseudodictyomitra lanceloti* Schaaf | |
| | *Suna hybum* (Foreman) | |
| | *Tethysetta boesii* (Parona) | |
| | *Thanarla pacifica* Nakaseko & Nishimura | |
| *Imamzadeh Village Section* | | |
| IR04-24 | *Cinguloturris fusiforma* Hori | Latest Oxfordian–Kimmeridgian |
| | *Emiluvia ordinaria* Ozvoldova | |
| | *Eucyrtidiellum ptyctum* (Riedel & Sanfilippo) | |
| | *Orbiculiforma*? *lowreyensis* Pessagno | |
| | *Pantanellium oligoporum* (Vinassa) | |
| | *Podocapsa amphitreptera* Foreman | |
| | *Protunuma japonicus* Matsuoka & Yao | |
| | *Pseudoeucyrtis reticularis* Matsuoka & Yao | |
| | *Ristola altissima altissima* (Rüst) | |
| | *Syringocapsa longituba* Steiger & Steiger | |
| | *Tetratrabs bulbosa* (Baumgartner) | |
| | *Williriedellum crystallinum* Dumitrica | |
| | *Zhamoidellum ovum* Dumitrica | |
| IR04-28 | *Archaeodictyomitra apiarium* (Rüst) | Late Kimmeridgian–early Tithonian |
| | *Emiluvia ordinaria* Ozvoldova | |
| | *Eucyrtidiellum ptyctum* (Riedel & Sanfilippo) | |
| | *Hsuum mclaughlini* Pessagno & Blome | |
| | *Mirifusus dianae dianae* (Karrer) | |
| | *Mirifisus dianae minor* (Baumgartner) | |
| | *Pantanellium oligoporum* (Vinassa) | |
| | *Podocapsa amphitreptera* Foreman | |
| | *Protunuma japonicus* Matsuoka & Yao | |
| | *Pseudoeucyrtis reticularis* Matsuoka & Yao | |
| | *Syringocapsa longituba* Steiger & Steiger | |
| | *Williriedellum crystallinum* Dumitrica | |
| | *Zhamoidellum ovum* Dumitrica | |
| IR04-29 | *Angulobracchia portmanni* Baumgartner | Late Tithonian–Berriasian |
| | *Archaeodictyomitra apiarium* (Rüst) | |
| | *Cinguloturris cylindra* Kemkin & Rudenko | |
| | *Emiluvia chica* (Foreman) | |
| | *Hiscocapsa kaminogoensis* (Aita) | |
| | *Pantanellium squinaboli* (Tan) | |
| | *Praeparvicingula cosmoconica* (Foreman) | |
| | *Svinitzium depressum* (Baumgartner) | |
| | *Tethysetta boesii* (Parona) | |
| IR04-33 | *Acaeniotyle umbilicata* (Rüst) | Latest Valanginian–Hauterivian |
| | *Cecrops septemporatus* (Parona) | |
| | *Crolanium* sp. | |
| | *Crucella bossoensis* Jud | |
| | *Dicerosaturnalis dicranacanthos* (Squinabol) | |

(*Continued*)

**Table 1.** *Continued*

| Sample | Radiolarians | Age |
|---|---|---|
| | *Dicerosaturnalis trizonalis* (Rüst) | |
| | *Hiscocapsa uterculus* (Parona) | |
| | *Mictyoditra pseudodecora* (Tan) | |
| | *Suna hybum* (Foreman) | |
| IR04-38 | *Archaeodictyomitra lacrimula* (Foreman) | Barremian |
| | *Aurisaturnalis carinatus perforatus* Dumitrica & Dumitrica-Jud | |
| | *Dicerosaturnalis dicranacanthos* (Squinabol) | |
| | *Dicerosaturnalis trizonalis* (Rüst) | |
| | *Cecrops septemporatus* (Parona) | |
| | *Hemicryptocapsa capita* (Tan) | |
| | *Mictyoditra* sp. | |
| | *Pantanellium* sp. | |
| | *Tethysetta boesii* (Parona) | |
| *Imamzadeh Negharek Khaneh Section* | | |
| IR04-43 | *Archaeocenosphaera*? *mellifera* O'Dogherty | Middle–late Albian |
| | *Holocryptocanium barbui* Dumitrica | |
| | *Mita gracilis* (Squinabol) | |
| | *Rhopalosyringium mosquense* (Smirnova & Aliev) | |
| IR04-14 | *Diacanthocapsa* sp. | Middle–late Albian |
| | *Dictyomitra montisserei* (Squinabol) | |
| | *Holocryptocanium barbui* Dumitrica | |
| | *Mita gracilis* (Squinabol) | |
| | *Mita obesa* (Squinabol) | |
| | *Mita spoletoensis* (O'Dogherty) | |
| | *Pseudodictyomitra lodogaensis* Pessagno | |
| | *Rhopalosyringium adriaticum* O'Dogherty | |
| | *Rhopalosyringium mosquense* (Smirnova & Aliev) | |
| IR04-18 | *Alievium* sp. | Turonian–Coniacian |
| | *Annikaella omanensis* De Wever, Bourdillon-de Grissac & Beurrier | |
| | *Archaeodictyomitra squinaboli* (Pessagno) | |
| | *Dictyomitra formosa* Squinabol | |
| | *Hemicryptocapsa polyhedra* Dumitrica | |
| | *Patellula verteroensis* (Pessagno) | |
| | *Theocampe ascaglia* Foreman | |
| | *Theocampe urna* (Foreman) | |

Dumitrica & Dumitrica-Jud 2005) indicates a late Bajocian age for the top of this cherty interval. *Unuma* cf. *typicus* Ichikawa & Yao in sample IR04-86, below, suggests that this sample is probably not older than the early Bajocian (FAD of *U. typicus* in UA Zone 3; i.e. the early–middle Bajocian). Sample IR04-97 from Bar Er contains typical Aalenian species such as *Elodium pessagnoi* Yeh & Cheng, *Hsuum altile* Hori & Otsuka, and *H. exiguum* Yeh & Cheng (see Gorican *et al.* 2006), together with *Parahsuum*? *natorense* (El Kadiri) (LAD in UA Zone 3).

In the overlying succession, thin chert is interbeded within calcareous turbidites and only rarely contains determinable radiolarians (Fig. 3, 16–18). A latest Bajocian–early Bathonian age (UA Zone 5) was determined on the basis of *Williriedellum tetragonum* (Matsuoka) in samples IR04-94 (Darreh Juve) and IR03-03 (Bar Er).

Callovian to early Oxfordian (UA Zones 7 and 8) radiolarians were obtained from the top of the Darreh Juve Formation in the Darreh Juve and Bar Er sections. The most characteristic species, which last occurs in UA Zone 7, is *Striatojaponocapsa conexa* (Matsuoka), which is abundant in sample IR04-130 (Fig. 3, 19–28) and is also present in sample IR04-131. In sample IR04-133 and in the correlative sample IR04-109 from Bar Er, only long-ranging species occur. However, the absence of *Striatojaponocapsa conexa* suggests that these two samples are younger (i.e. probably assignable to UA Zone 8; middle Callovian–early Oxfordian).

Middle–late Oxfordian to mid-Tithonian radiolarians (UA Zones 9–12; Fig. 4, 1–13) were found in the proximal successions of the Imamzadeh Formation in the Imamzadeh sections. The oldest sample, IR04-49, already contains *Emiluvia ordinaria* Ozvoldova, which first appears in UA Zone 9 (mid–late Oxfordian). *Williriedellum crystallinum* Dumitrica was also identified. *Podocapsa amphitreptera* Foreman was the most characteristic species in the following samples: IR04-53 to 56 and IR04-24 to 28. Other species, not extending above UA Zone 11 (late Kimmeridgian–early Tithonian), are found together in sample IR04-28; for example *Emiluvia ordinaria* Ozvoldova, *Pseudoeucyrtis reticularis* Matsuoka & Yao and *Eucyrtidiellum ptyctum* (Riedel & Sanfilippo). Sample IR04-56 contains *Cinguloturris cylindra* Kemkin & Rudenko, *Eucyrtidiellum pyramis* (Aita) and *Ristola cretacea* (Baumgartner), together with *Protunuma japonicus* Matsuoka & Yao and *Syringocapsa longituba* Steiger & Steiger (determined as *S. spinellifera* Baumgartner by Baumgartner *et al.* 1995), and is thus assigned to UA Zone 12 (early–early late Tithonian). *Podocapsa amphitreptera* starts in UA Zone 9 of Baumgartner *et al.* (1995), but is found somewhat later in other zonations (e.g. Gorican 1994). Sample IR04-49 lacks *P. amphitreptera* and is therefore assigned to middle–late Oxfordian. The overlying samples are from the latest Oxfordian to mid-Tithonian. Time-equivalent deposits of the distal successions from Darreh Juve and Bar Er are shales devoid of determinable radiolarians. The youngest Jurassic cherts of the proximal successions (sample IR04-56) are approximately correlative with the transition from shale to pure radiolarian chert in distal successions (see sample IR04-118, below).

Late Tithonian to Aptian radiolarian assemblages were obtained from both the proximal and distal successions. In both settings, the radiolarians are relatively well preserved throughout the sections. In this time interval, three major radiolarian turnovers occur around the following horizons: early–late Valanginian, Hauterivian–Barremian and early–middle Aptian (Jud 1994; O'Dogherty 1994; O'Dogherty & Guex 2002). It is therefore relatively easy to divide this interval into three main assemblages.

The lowest assemblage (i.e. late Tithonian to early Valanginian; Fig. 4, 14–26) is characterized by the first appearance of *Angulobracchia portmanni* Baumgartner, *Paronaella*? *tubulata* Steiger, *Praeparvicingula cosmoconica* (Foreman) and *Svinitzium depressum* (Baumgartner) in UA Zone 13 of Baumgartner *et al*. (1995), and corresponds to zones D1 to base D2 of Jud (1994). Therefore, samples IR04-29, IR04-57 and IR04-137 are certainly at least late Tithonian in age. For sample IR04-118, the distinction between early and late Tithonian is not possible because *Paronaella*? *tubulata* Steiger (FAD in UA Zone 13) coexists with *Protunuma japonicus* Matsuoka & Yao and *Syringocapsa longituba* Steiger & Steiger (both LAD in UA Zone 12). Late Tithonian to early Valanginian radiolarians were recovered from pure radiolarian cherts in the Darreh Juve and Bar Er sections (samples IR04-137 to 142 and IR04-120). The common species in this earliest Cretaceous assemblage is also *Cinguloturris cylindra* Kemkin & Rudenko, which does not extend above the Valanginian.

The most distinctive species in the second early Cretaceous assemblage (Fig. 5, 1–15) is *Cecrops septemporatus* (Parona), which ranges from the late Valanginian to the Barremian (zones E2–G1 of Jud 1994). It is also important to note the simultaneous first appearance of *Crolanium* spp. (zone E2) and somewhat later appearance of *Suna hybum* (Foreman) (zone F1). This assemblage was found in the Imamzadeh sections (samples IR04-70 and IR04-33) and at Darreh Juve (IR04-146). *Aurisaturnalis variabilis* (Squinabol), ranging from the latest Valanginian to the late Hauterivian (zones F1–F3) is common in samples IR04-70 and IR04-146.

The latest Hauterivian to early Aptian (Fig. 5, 6–11) is characterized by *Aurisaturnalis carinatus* (Foreman), which rapidly evolved from *Aurisaturnalis variabilis* (Squinabol) across the Hauterivian–Barremian boundary and became extinct in the early Aptian (Dumitrica & Dumitrica-Jud 1995). The transitional subspecies are very rare around the boundary level; however, the advanced subspecies *A. carinatus perforatus* Dumitrica & Dumitrica-Jud is more common, easily recognizable and very useful stratigraphically. This subspecies first appears near the top of the Barremian G1 zone (Dumitrica & Dumitrica-Jud 1995). The assemblage further contains many species that became extinct either during the early Aptian [e.g. *Tethysetta boesii* (Parona), *Tethysetta usotanensis* (Tumanda), *Mictyoditra pseudodecora* (Tan)] or the earliest middle Aptian (e.g. *Archaeodictyomitra lacrimula* (Foreman), *Suna hybum* (Foreman), *Thanarla pacifica* Nakaseko & Nishimura, *Pantanellium* spp.) (see O'Dogherty 1994). The following samples are assigned to this interval: IR04-72 and IR04-38 from the Imamzadeh sections, IR04-121 from Bar Er, and IR04-147 to IR04-151 from Darreh Juve. In sample IR04-38, the coexistence of *Cecrops septemporatus* (Parona) and *Aurisaturnalis carinatus perforatus* Dumitrica & Dumitrica-Jud allows a more precise age assignment to the Barremian (i.e. zone G1 of Jud 1994; see Dumitrica & Dumitrica-Jud 1995). In the Darreh Juve samples, the latest Hauterivian to early Aptian interval is well documented across a succession more than 50 m thick. Thus, it seems likely that the upper sample

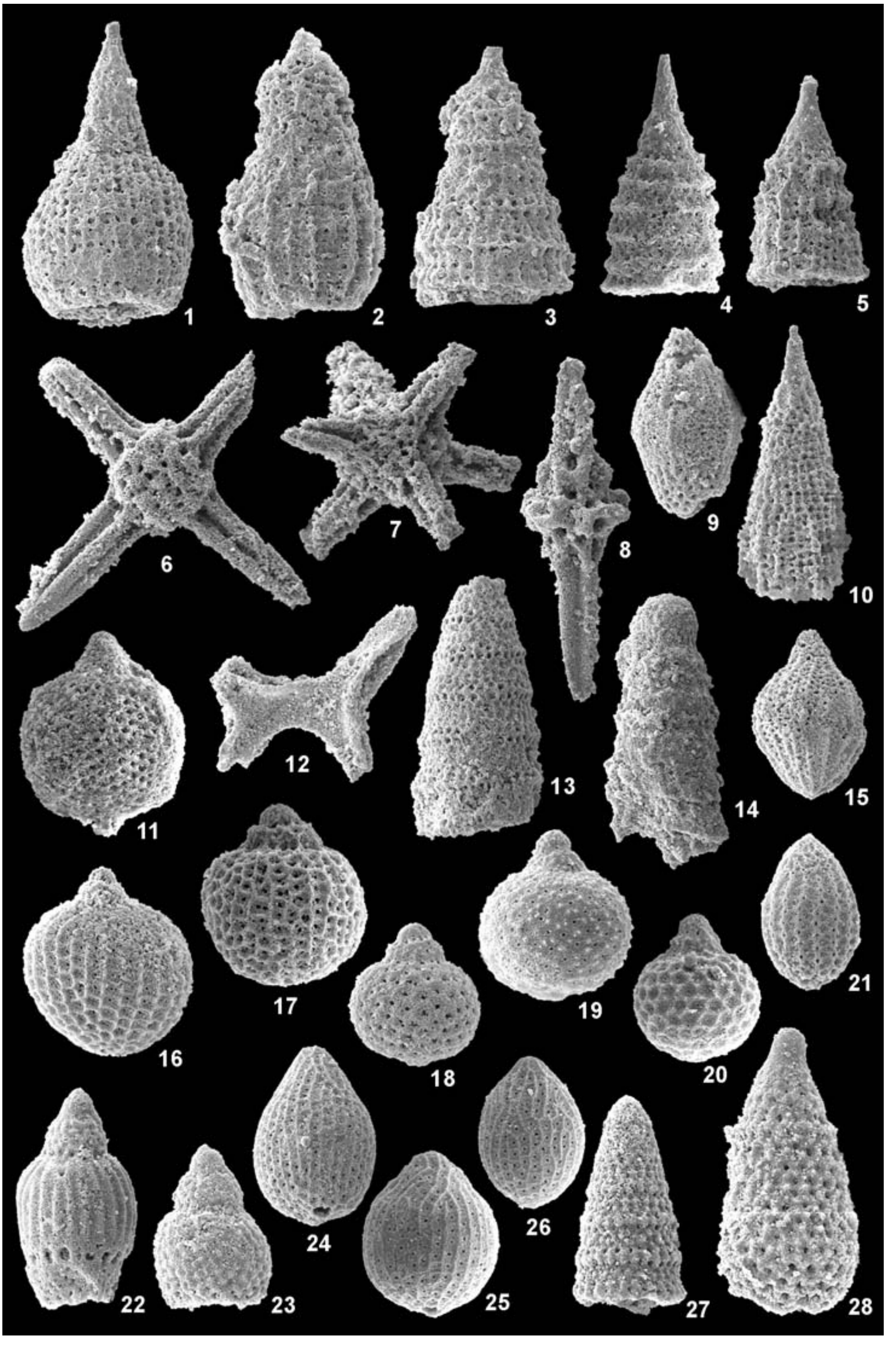


**Fig. 3.** Middle Jurassic radiolaria from the Bar Er and Dareh Juve sections. The sample number, SEM number and magnification are indicated for each illustration. 1, *Parahsuum? natorense* (El Kadiri), IR04-97, 071702, 150×. 2, *Hsuum altile* Hori & Otsuka, IR04-97, 071711, 200×. 3, *Elodium pessagnoi* Yeh & Cheng, IR04-97, 071708, 200×. 4, *Praeparvicingula nanoconica* (Hori & Otsuka), IR04-97, 071706, 200×. 5, *Hsuum exiguum* Yeh & Cheng, IR04-97,

(IR04-151) is early Aptian in age. The highest productive sample of this section (IR04-153) contains a poorly preserved radiolarian assemblage. The only stratigraphically important species is *Archaeodictyomitra lacrimula* (Foreman), whose range does not extend above the base of the middle Aptian (base of Costata subzone according to O'Dogherty 1994).

Late Aptian and early Albian radiolarians were not recovered from the studied sections. Sediments of this age are apparently missing, either because the upper boundary of the Imamzadeh Formation is erosional or the succession is truncated by a fault on the top. Middle–late Albian radiolarians (Fig. 5, 19–26) were found in samples IR04-43 and IR04-14, both below and above a thick conglomerate with boulders at Negareh-Khaneh (i.e. the lower member of the Neghareh Khaneh Formation). The age is constrained by *Archaeocenosphaera*? *mellifera* O'Dogherty, *Mita gracilis* (Squinabol), *Rhopalosyringium mosquense* (Smirnova & Aliev), which first occur in the middle Albian, and by *Mita spoletoensis* (O'Dogherty), which is the index taxon of the Spoletoensis zone (middle Albian to the base of the Cenomanian; O'Dogherty 1994). The highest sample of this section (IR04-18, the upper member from the Neghareh Khaneh Formation) (Fig. 5, 19–26) contains *Hemicryptocapsa polyhedra* Dumitrica, which is a typical Turonian species (O'Dogherty 1994). On the other hand, it also contains *Theocampe urna* (Foreman) and the genus *Annikaella*, both known to occur from the Coniacian onward (Sanfilippo & Riedel 1985; De Wever *et al.* 1988; see also Dumitrica *et al.* 1997, p. 15). Because O'Dogherty's zonation extends only to the early Turonian and because an accurate radiolarian zonation is not available for the successive stages, the age of sample IR04-18 is broadly determined as Turonian–Coniacian.

Not a single radiolarian, either *in situ* or reworked, was found in the shales of the Bar Er Fm.

The oldest age obtained for the Darreh Juve Fm is Aalenian–early Bajocian? (in the Bar Er section). The youngest age is middle Callovian–early Oxfordian (in the Darreh Juve and Bar Er sections).

The base of the Imamzadeh Fm is middle–late Oxfordian (Imamzadeh–Lake Bakhtegan section). The boundary between the two members (i.e. the lower and upper) is diachronous, from early–early late Tithonian (Imamzadeh–Lake Bakhtegan) to late Tithonian–early Valanginian (Bar Er section). The top of the Imamzadeh Fm is at least early Aptian in age.

The lower member of the Neghareh-Khaneh Fm, primarily made of coarse-grained sediments, is poor in radiolarians, with a middle–late Albian age on top. It might be late Aptian?–Albian in age. Its upper member is of Albian (late?) to Turonian–Coniacian age, although it could be younger.

## Sedimentology: facies description

In this study, 27 facies are described throughout the measured sections. These are grouped into eight major facies associations (see Fig. 6 for description and Fig. 7 for photographs). All of these facies are typical gravity-flow deposits, according to the classification of Mutti (1992). However, one group of facies, here named 'slaty' medium-grained sands, is specific to this study (not included in the study by Mutti 1992). The eight main facies associations are defined from the grain size of the sediments, their homolithic or heterolithic characters, and, in two cases, their sedimentary structures.

The two first associations (C.ms and C.cs, Figs 6 & 7a, b) are coarse-grained, conglomeratic sediments, either matrix- or clast-supported. The petrology and shape of both the matrix particles and the clasts are highly variable (either rounded or angular). If rounded, the pebbles are part of clast-supported conglomerates and vice versa. The matrix of the bimodal matrix-supported conglomerates ranges from small angular to subangular pebbles to carbonate silts. In the case of the conglomerates,

**Fig. 3.** (*Continued*) 071704, 200×. 6, *Tympaneides* sp., IR04-86, 071604, 200×. 7, *Thurstonia* sp., IR04-86, 071606, 200×. 8, *Trillus* sp., IR04-86, 071607, 200×. 9, *Unuma* cf. *typicus* Ichikawa & Yao, IR04-86, 071613, 200×. 10, *Hsuum* cf. *matsuokai* Isozaki & Matsuda, IR04-86, 071611, 200×. 11, *Williriedellum marcucciae* Cortese, IR04-89, 071508, 250×. 12, *Hexasaturnalis suboblongus* (Yao), IR04-89, 071502, 250×. 13, *Dictyomitrella*? *kamoensis* Mizutani & Kido, IR04-89, 071513, 250. 14, *Stichomitra*? *takanoensis* Aita, IR04-89, 071514, 200×. 15, *Protunuma fusiformis* Ichikawa & Yao, IR04-89, 071510, 200×. 16, *Williriedellum tetragonum* (Matsuoka), IR04-94, 071313, 250×. 17, *Williriedellum* aff. *tetragonum* (Matsuoka), IR04-94, 071306, 250×. (Note that some frames include more than one pore.) 18, *Williriedellum yaoi* (Kozur), IR04-94, 071308, 250×. 19, *Williriedellum* cf. *yaoi* (Kozur) (corroded specimen), IR04-130, 070416, 250×. 20, *Williriedellum yaoi* (Kozur), IR04-130, 070415, 250×. 21, *Plicaforacapsa catenarum* (Matsuoka), IR04-130, 070406, 250×. 22, *Eucyrtidiellum ptyctum* (Riedel & Sanfilippo), IR04-130, 070408, 250×. 23, *Eucyrtidiellum nodosum* Wakita, IR04-130, 070417, 250×. 24–26, *Striatojaponocapsa conexa* (Matsuoka), IR04-130 (24, 070427; 25, 070430; 26, 070435) 250×. 27, *Dictyomitrella*? *kamoensis* Mizutani & Kido, IR04-130, 070420, 250×. 28, *Pseudoristola tsunoensis* (Aita), IR04-130, 070407, 250×.

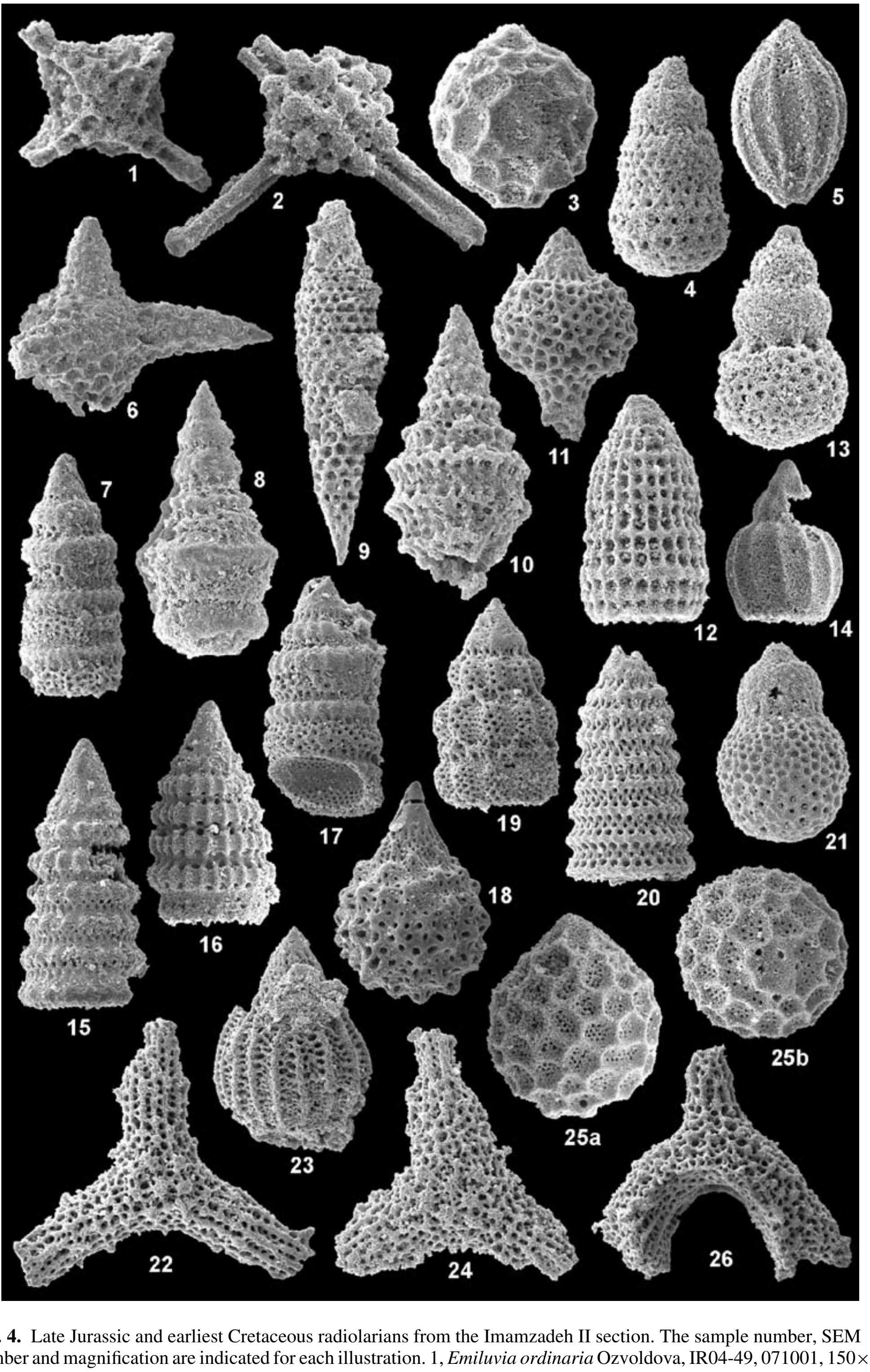


**Fig. 4.** Late Jurassic and earliest Cretaceous radiolarians from the Imamzadeh II section. The sample number, SEM number and magnification are indicated for each illustration. 1, *Emiluvia ordinaria* Ozvoldova, IR04-49, 071001, 150×. 2, *Emiluvia orea* Baumgartner, IR04-49, 071003, 150×. 3, *Williriedellum crystallinum* Dumitrica, IR04-49, 071005, 200×. 4, *Sethocapsa* aff. *horokanaiensis* Kawabata, IR04-49, 071018, 250×. 5, *Protunuma japonicus* Matsuoka & Yao,

the nature of the source area seems to be of primary importance, more so than the process itself (i.e. debris flows v. high-density turbidity current; Shanmugam 1996, 2000). For the rounded clast-supported conglomerates, the source seems to be pebbles rounded by waves on the shore or in rivers in an upstream catchment, and all of the fine-grained particles have been winnowed. For the subangular to angular matrix-supported conglomerates, the pebbles come from a local relief: they mixed with the overlying soft sediments and were transported toward the basin during a single episode from this source by gravity flows.

The third association (Sc.meg, Fig. 6) is made up of coarse-grained sands with possible granules and megaripples. It corresponds to the classical Mutti's by-pass facies (e.g. F6, Mutti, 1979, 1992).

The fourth association (Sc, Figs 6 & 7c), which is the most common of the homolithic facies, is characterized by poorly sorted coarse-grained sands. All of the intermediates between bimodal and unimodal sands exist from granule-rich sands (bimodal) to poorly sorted sands (unimodal). Both are mostly structureless. Some planar laminations can occur in the unimodal sands. The exact nature of the related transport process is difficult to determine (debris flows v. high-density turbidity current).

The fifth association (Sm.sl, Figs 6 & 7d) is specific to the southern Tethys margin (these facies also develop along the Oman palaeomargin). These facies, which are either homolithic or heterolithic, are composed of stacked subplanar lamina-sets with a thickness of a few centimetres. These lamina-sets may be planar, but generally they are slightly undulating (subplanar laminations). In some cases, the undulation amplitude is high enough to generate structures similar to growing hummocky cross-stratification (HCS; Bourgeois 1983; Fig. 7e). They differ from a true HCS by their grain size (which is coarser than the very well-sorted fine to medium sands from the storm-induced HCS) and the lack of an association with true wave ripples. The significance of the lamina-sets is unclear: they may represent flow velocity variations or amalgamated deposits of distinct gravity flows. They can be bundled into bedsets that could record different stacked depositional events. The process of transport and deposition is difficult to determine: the subplanar lamination and the growing HCS suggest a deposition from a suspension (i.e. the draping of vertically growing structures), but the occurrence of parting lineation on the planar laminations indicates a dominant bedload component (Harms 1975; Allen 1982).

The sixth and the seventh associations (Sm.he1, Sm.he2, Fig. 6) represent classical turbiditic facies (i.e. medium-density turbidity flows) that can be described using the classical Bouma model (Bouma 1962). The planar laminations include two distinct subfacies: the first is characterized by true graded laminations and the second by crude planar (subplanar) laminations. This latter subfacies corresponds to the distal equivalent of facies association Sm.sl. Two types of current ripple bedding are recognized: strictly bedload and a mixed bedload–suspended load (type A and B climbing ripples; Allen 1973). The subfacies with bedload current ripples is rare and seems to be a local record of facies association Sm.sl.

The eighth association (Sf.he, Figs 6 & 7f) is composed of fine-grained thin layers (a few centimetres thick), with either planar to subplanar laminations or undulating laminations (from HCS-like structures to in-phase current climbing ripples; type S of Allen 1973). They correspond to low-density turbidity currents. No true Stow sequences (Shanmugam 2000) were encountered. Based on petrology, two sub-associations can be defined: carbonate and siliceous (radiolarians). In the study area, radiolarians behave as particles and are reworked, transported and deposited under the action of gravity turbulent flows. They show evidence of grading and laminations, with the existence of ripple undulations on top of the strata.

**Fig. 4.** (*Continued*) IR04-56, 071222, 200×. 6, *Podocapsa amphitreptera* Foreman, IR04-53, 071103, 150×. 7, *Cinguloturris cylindra* Kemkin & Rudenko, IR04-56, 071201, 200×. 8, *Cinguloturris fusiforma* Hori, IR04-56, 071241, 200×. 9, *Pseudoeucyrtis reticularis* Matsuoka & Yao, IR04-53, 071128, 150×. 10, *Tethysetta mashitaensis* (Mizutani), IR04-53, 071108, 150×. 11, *Syringocapsa longituba* Steiger & Steiger, IR04-56, 071221, 150×. 12, *Archaeodictyomitra apiarium* (Rüst), IR04-56, 071211, 200×. 13, *Sethocapsa horokanaiensis* Kawabata, IR04-56, 071233, 250×. 14, *Eucyrtidiellum pyramis* (Aita), IR04-57, 070227, 200×. 15, *Pseudodictyomitra carpatica* (Lozyniak), IR04-57, 070324, 200×. 16, *Svinitzium depressum* (Baumgartner), IR04-57, 070207, 200×. 17, *Cinguloturris cylindra* Kemkin & Rudenko, IR04-57, 070206, 150×. 18, *Fultacapsa tricornis* (Jud), IR04-57, 070224, 150×. 19, *Neorelumbra tippitae* Kiessling, IR04-57, 070215, 150×. 20, *Praeparvicingula cosmoconica* (Foreman), IR04-57, 070213, 150×. 21, *Tricolocapsa*? *campana* Kiessling, IR04-57, 070241, 200×. 22, 24, *Paronaella*? *tubulata* Steiger, IR04-57 (22, 070312; 24, 070317), 150×. (Note tritrabid structure on distal extension of arms.) 23, *Hsuum raricostatum* Jud, IR04-57, 070221, 150×. 25a and b, *Williriedellum* aff. *crystallinum* Dumitrica, IR04-57 (25a, 070229; 25b, 070230, antapical view showing closed aperture with three pores), 200×. 26, *Deviatus diamphidius* (Foreman), IR04-57, 070304, 150×.

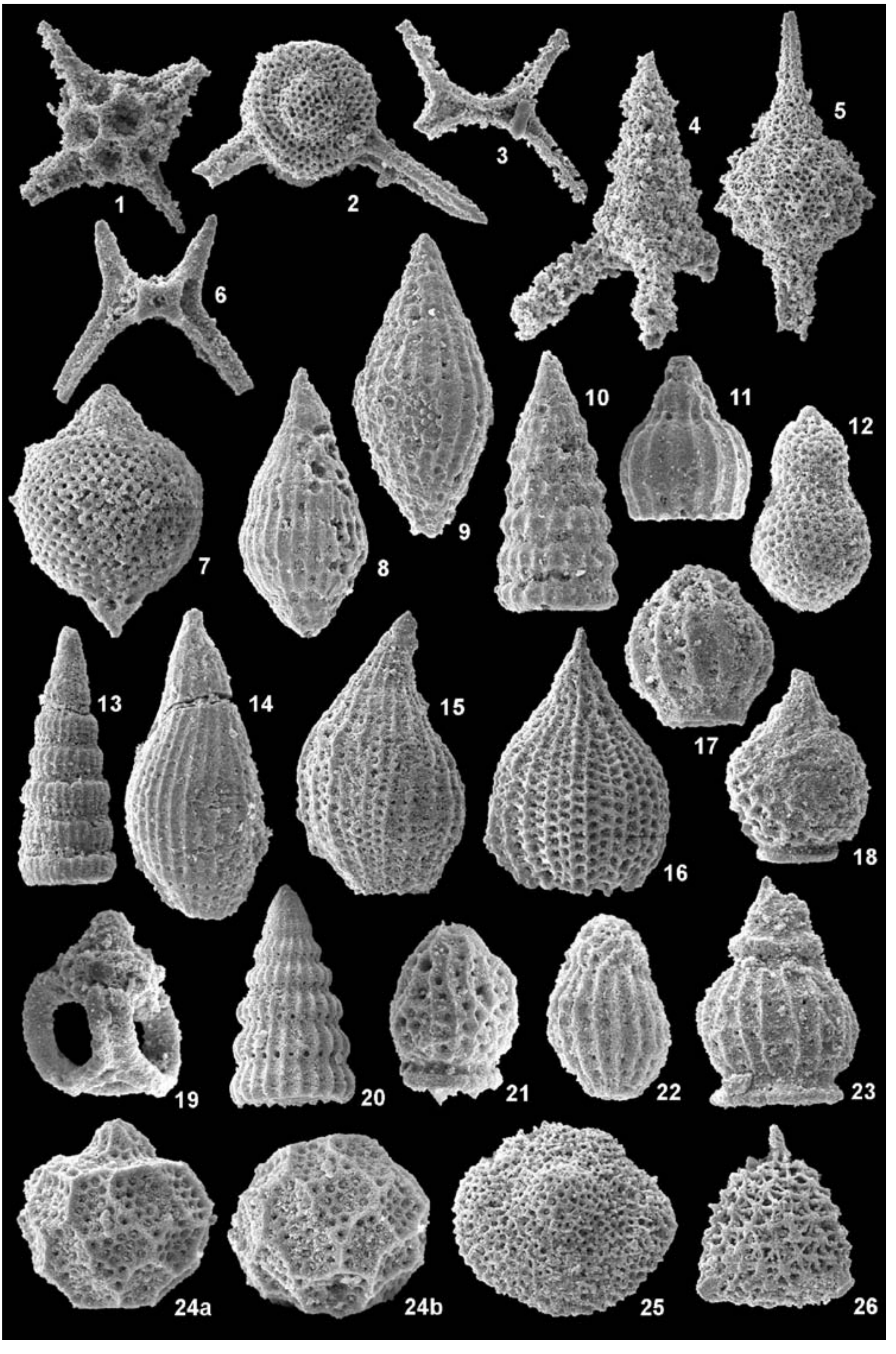


**Fig. 5.** Cretaceous radiolarians from the Imamzadeh, Dareh Juve and Negareh-Khaneh sections. The sample number, SEM number and magnification are indicated for each illustration. 1, *Cecrops septemporatus* (Parona), IR04-70, 070901, 200×. 2, *Suna hybum* (Foreman), IR04-70, 070911, 150×. 3, *Aurisaturnalis variabilis variabilis* (Squinabol), IR04-70, 070905, 200×. 4, *Crolanium bipodium* (Parona), IR04-70, 070923, 200×. 5, *Syringocapsa limatum* Foreman,

In the field, along cliffs, sometimes with an exposure a few kilometres long, most of the deposits are laterally continuous with minor changes in facies and thicknesses, which correspond to lobe deposits. Channel structures have been recognized in the Darreh Juve Formation. They correspond to low erosional structures (maximum depth 1 m) with a width ranging from tens to hundreds of metres. A deeply incised channel (canyon?), filled by conglomerates and blocks, was identified in the Lower Member of the Neghareh Khaneh Formation. The few occurring slumps are *in situ* slumps with a low horizontal displacement (a few metres) on a local décollement level.

## Discussion: facies model

### *Facies zonation (Fig. 8)*

As mentioned above, the main objective of this sedimentological study was to establish a proximal–distal facies zonation to define the main discontinuities in the deep-sea sedimentary record of the southern Tethyan passive margin in Iran. However, field data are not abundant enough to construct precise 3D geometries of these gravity-flow systems. The main difficulty of this exercise is to take into account the lateral substitution of two or more facies that, with time, can be deposited at the same place along the depositional profile. The model proposed here was based on hydrodynamical considerations (i.e. the same type of processes and flow velocity) and on field data (i.e. rare lateral variations on outcrops and the close vertical association of two facies in a given area).

Coarse-grained sands with a megaripple facies association (the sc.meg or F6 by-pass facies of Mutti 1992) are closely associated (Fig. 8) with the coarse-grained sand facies association (Cs). They record the transition between the two types of gravity-flow systems (Mutti 1992; Mutti *et al.* 1999). Conglomeratic facies associations (C.ms, C.cs), with evidence of channels, are located upstream of this by-pass facies association (Cs.meg). The conglomeratic facies associations (C.ms, C.cs) were not ranked along the profile: they record changes in the lithology of the source area, rather than any proximal–distal trends (see discussion, below).

Downstream, lobe deposits start with thick homolithic coarse-grained sands (Sc). They can laterally pass into two types of facies successions (Fig. 8): (1) the ‘classical’ Bouma sequence evolution (Sm.he) or (2) the ‘slaty’ facies evolution (Sm.sl). Discerning the reason for the two types of evolution is not an aim of this study. However, a possible explanation could be a change in carbonate production on the platform and then a change in the sediment grain sizes (i.e. poorly sorted coarse-grained sands v. better sorted medium-grained sands). The Bouma sequence evolution (Sm.he) displays a classical lateral evolution with Ta to Tab sequences upstream and Tc downstream. The ‘slaty’ facies evolution (Sm.sl) shows a more complex pattern with a more ‘planar to subplanar lamination’ trend (the most common) and an ‘HCS-like’ trend (Fig. 8).

The distal transition toward fine-grained sand facies (Sf.he) is unclear: this does not correspond to the classical evolution through space of the Bouma sequence. The strata, made of Tc sequences (Sm.he2), are laterally continuous and are interbedded with Sf.he strata. The grain size and the sedimentary structures of the Sf.he strata are more compatible with a lateral evolution from the ‘slaty’ facies (Sm.sl) trend. This is supported by the same high-frequency rate of gravity-flow event preservation for both the Sm.sl and the Sf.he facies associations.

Two laterally equivalent trends have been defined. The Bouma sequence evolution passes from massive structureless beds to planar (subplanar) laminated strata and then to in-phase climbing current ripple beddings. The ‘slaty’ facies evolution evolves from Sm.sl facies associations to

**Fig. 5.** (*Continued*) IR04-70, 070921, 150×. 6, *Aurisaturnalis carinatus perforatus* Dumitrica & Dumitrica-Jud, IR04-38, 070703, 200×. 7, *Hemicryptocapsa capita* (Tan), IR04-38, 070711, 200×. 8, 9, *Archaeodictyomitra lacrimula* (Foreman), IR04-151 (8, 070814; 9, 070809), 200×. 10, *Pseudodictyomitra* cf. *carpatica* (Lozyniak), IR04-151, 070822, 200×. 11, *Thanarla pacifica* Nakaseko & Nishimura, IR04-151, 070831, 200×. 12, *Diacanthocapsa* sp., IR04-14, 070625, 200×. 13, *Pseudodictyomitra lodogaensis* Pessagno, IR04-14, 070637, 200×. 14, *Mita gracilis* (Squinabol), IR04-14, 070614, 200×. 15, *Mita obesa* (Squinabol), IR04-14, 070606, 150×. 16, *Mita spoletoensis* (O’Dogherty), IR04-14, 070602, 150×. 17, *Rhopalosyringium adriaticum* O’Dogherty, IR04-14, 070619, 300×. 18, *Rhopalosyringium mosquense* (Smirnova & Aliev), IR04-14, 070618, 200×. 19, *Annikaella omanensis* De Wever, Bourdillon-de Grissac & Beurrier, IR04-18, 070503, 300×. 20, *Dictyomitra formosa* Squinabol, IR04-18, 070502, 200×. 21, *Theocampe* sp., IR04-18, 070505, 300×. 22, *Theocampe ascalia* Foreman, IR04-18, 070508, 300×. 23, *Theocampe urna* (Foreman), IR04-18, 070504, 300×. 24a and b, *Hemicryptocapsa polyhedra* Dumitrica, IR04-18 (24a, 070510; 24b, 070511, antapical view), 300×. 25, *Patellula verteroensis* (Pessagno), IR04-18, 070522, 150×. 26, *Alievium* sp., IR04-18, 070519, 150×.

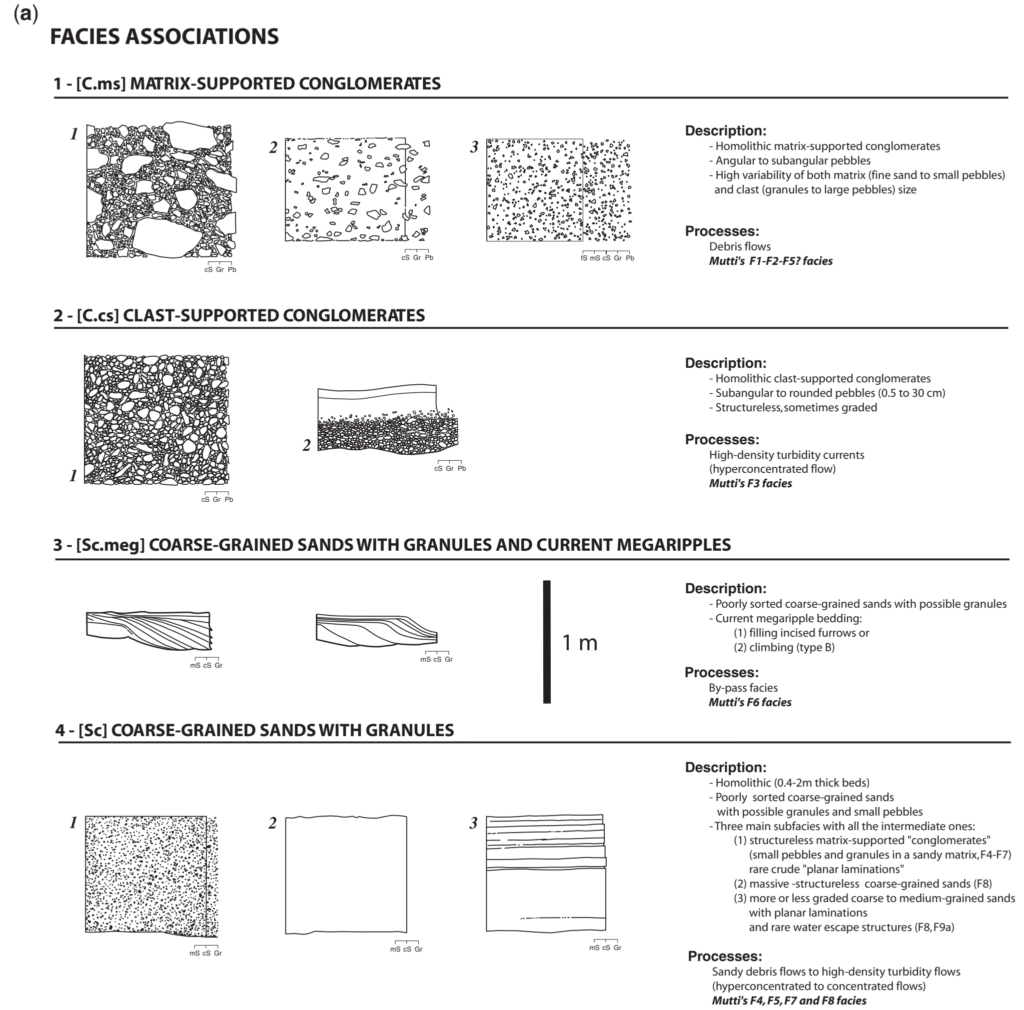


**Fig. 6.** Facies and facies associations: description and interpretation.

most of the Sf.he facies, including carbonate strata upstream and siliceous (radiolaritic) strata downstream. The radiolaritic facies may laterally replace the distal carbonate silt layers. The significance of the radiolarite facies evolution, including the type of the source area, is not understood.

## *Palaeocurrent data and palaeotopographic implications*

Palaeocurrent measurements were taken from both the Darreh Juve and Imamzadeh Formations (Fig. 9). For the Darreh Juve Formation (Aalenian–Callovian), all three sections (i.e. Imamzadeh–Lake Bakhtegan, Darreh Juve and Bar Er) show the same dominant pattern toward the NW quarter: Imamzadeh–Lake Bakhtegan is NW dominant, with some WSW and ENE directions; Darreh Juve is west dominant, with some east and north directions; and Bar Er is WNW dominant, with NNW and north directions. However, other directions can exist, sometimes at 180° to each other. This can imply either a multisource system, indicating a complex topography of the platform, or a reflection of turbidity currents on the opposite slopes of a relatively narrow basin (Pickering & Hiscott 1985; Kneller *et al.* 1991).

The palaeocurrent pattern is more complex for the Imamzadeh Formation (Oxfordian–Aptian): Imamzadeh–Lake Bakhtegan is NNW dominant, with an ESE direction; Imamzadeh village is SE

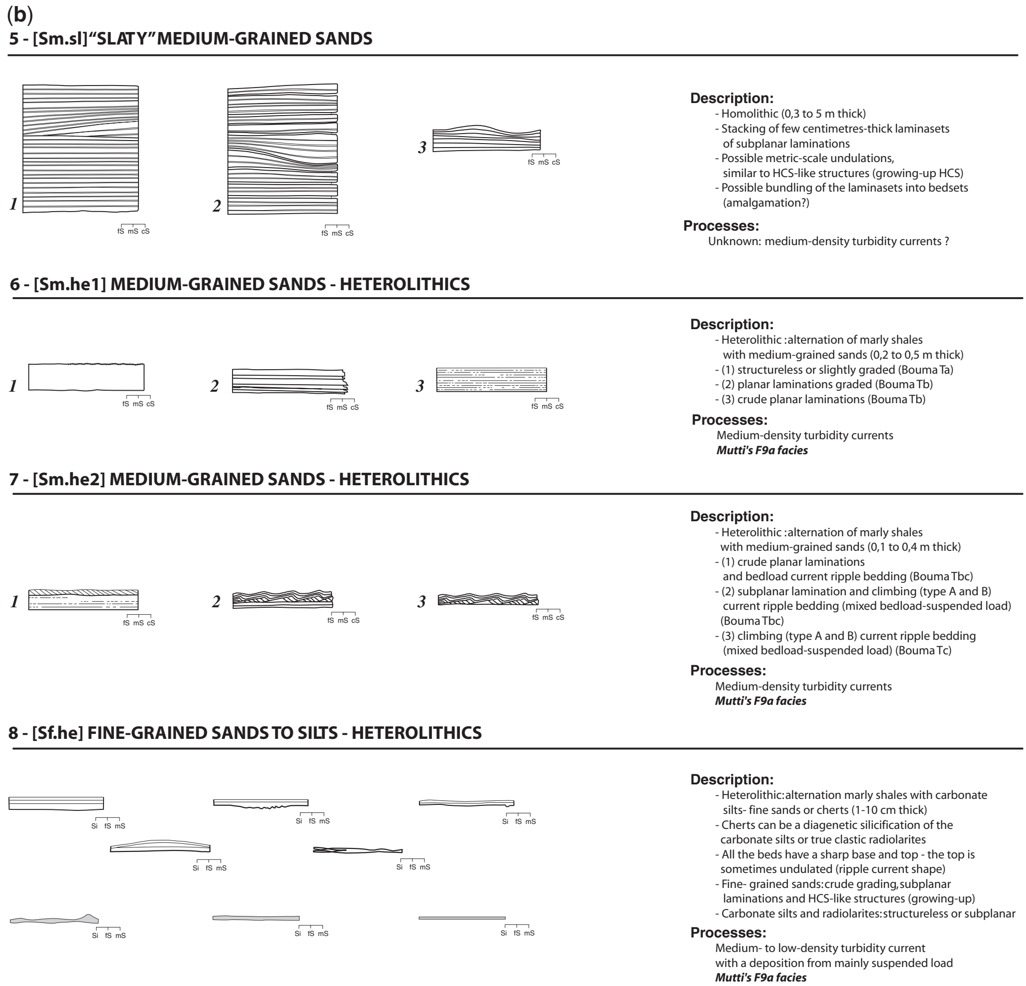


**Fig. 6.** (*Continued*)

dominant, with north and south directions; Darreh Juve is WNW dominant, with an east direction; and Bar Er is WNW dominant. The SE directions of the Imamzadeh village section could be explained by tectonic rotation, but because the SE directions are at 180° to the other NW dominant directions, the best explanation for this SE-dominant direction is again either multisource systems on opposite platforms or reflected turbidity currents.

These palaeocurrent measurements suggest a complex topographic pattern in the basin with a narrow (100 km large) deep-sea system. This is in good agreement with the palaeogeographical data provided by Murris (1980) and Ziegler (2001), and the idea of isolated carbonate platforms (so-called seamounts) close to the transition between continental and oceanic crust.

## Sequence stratigraphy: correlations

Five major stratigraphic cycles were identified and correlated along the five measured sections (Fig. 10). Two cycles have been defined for the Jurassic (labelled J2 and J3) and three for the lower Cretaceous (labelled K1.1, K1.2 and K1.3). The undated base of the Bar Er Formation records an overall distal-up trend, with a maximum of distal facies (Fig. 10) on top of the formation.

Based on biochronostratigraphic data, the order of magnitude of duration of these five major cycles is around 10 Ma, which corresponds to second-order cycles. At a lower time-scale duration, cycles lasting a few million years (i.e. third-order cycles) can be defined. The resolution of the biostratigraphic data is not sufficient to validate

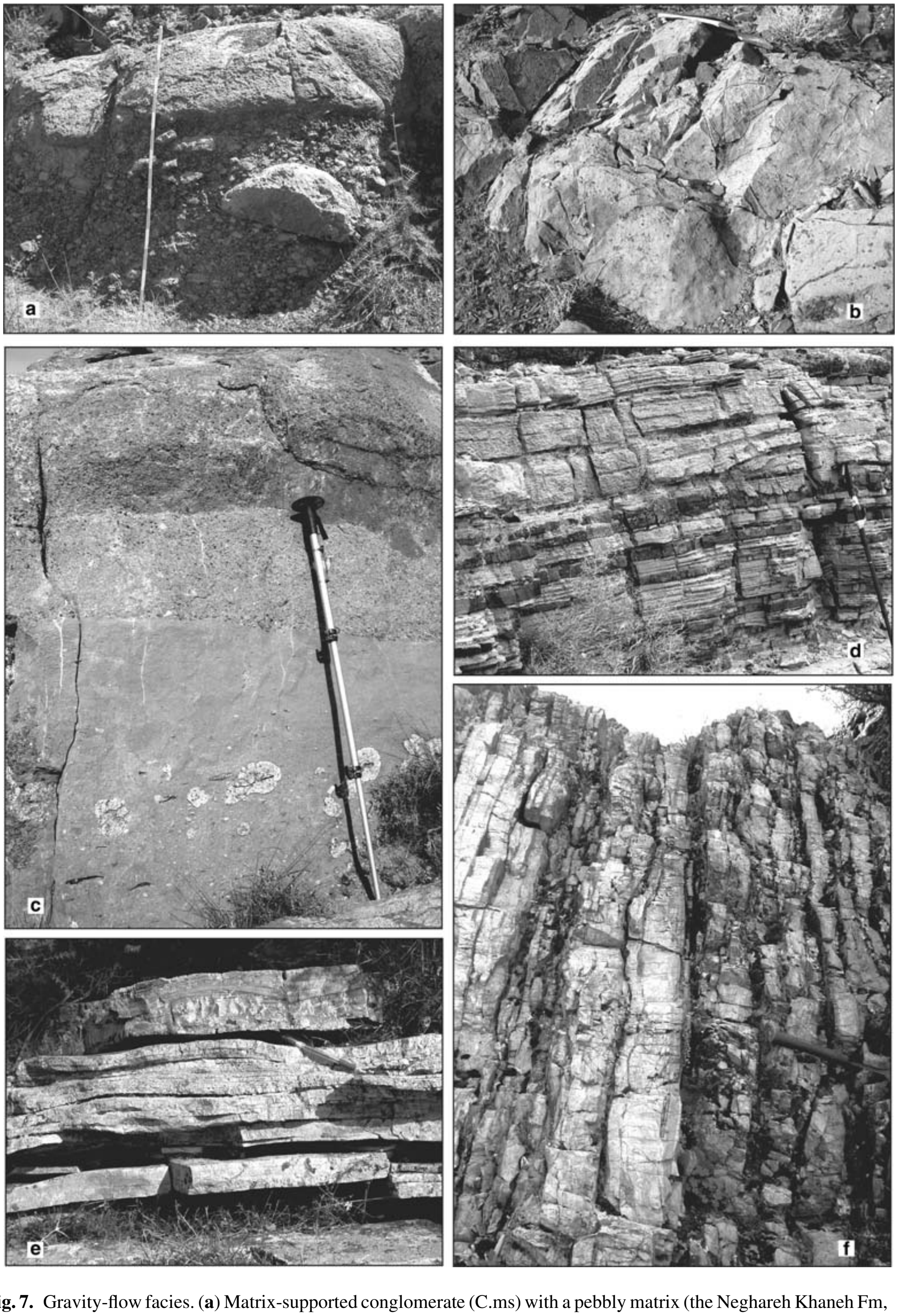

**Fig. 7.** Gravity-flow facies. (**a**) Matrix-supported conglomerate (C.ms) with a pebbly matrix (the Neghareh Khaneh Fm, lower member, Imamzadeh–Neghareh Khaneh section). (**b**) Matrix-supported conglomerate (C.ms) with a matrix of fine-grained carbonate sands (the Darreh Juve Fm, Bar Er section). (**c**) Massive coarse-grained carbonate sands with granules and/or small pebbles (Sc) (the Imamzadeh Fm, Imamzadeh Village). (**d**) 'Slaty' (Sm.sl) medium-grained carbonate sands (the Imamzadeh Fm, Imamzadeh–Lake Bakhtegan). (**e**) Growing HCS-like structure (Sm.sl to Sf.he) in heterolithic fine- to medium-grained carbonate sands (the Imamzadeh Fm, Imamzadeh Village). (**f**) Radiolarites (Sf.he) (the Imamzadeh Fm, Imamzadeh Village).

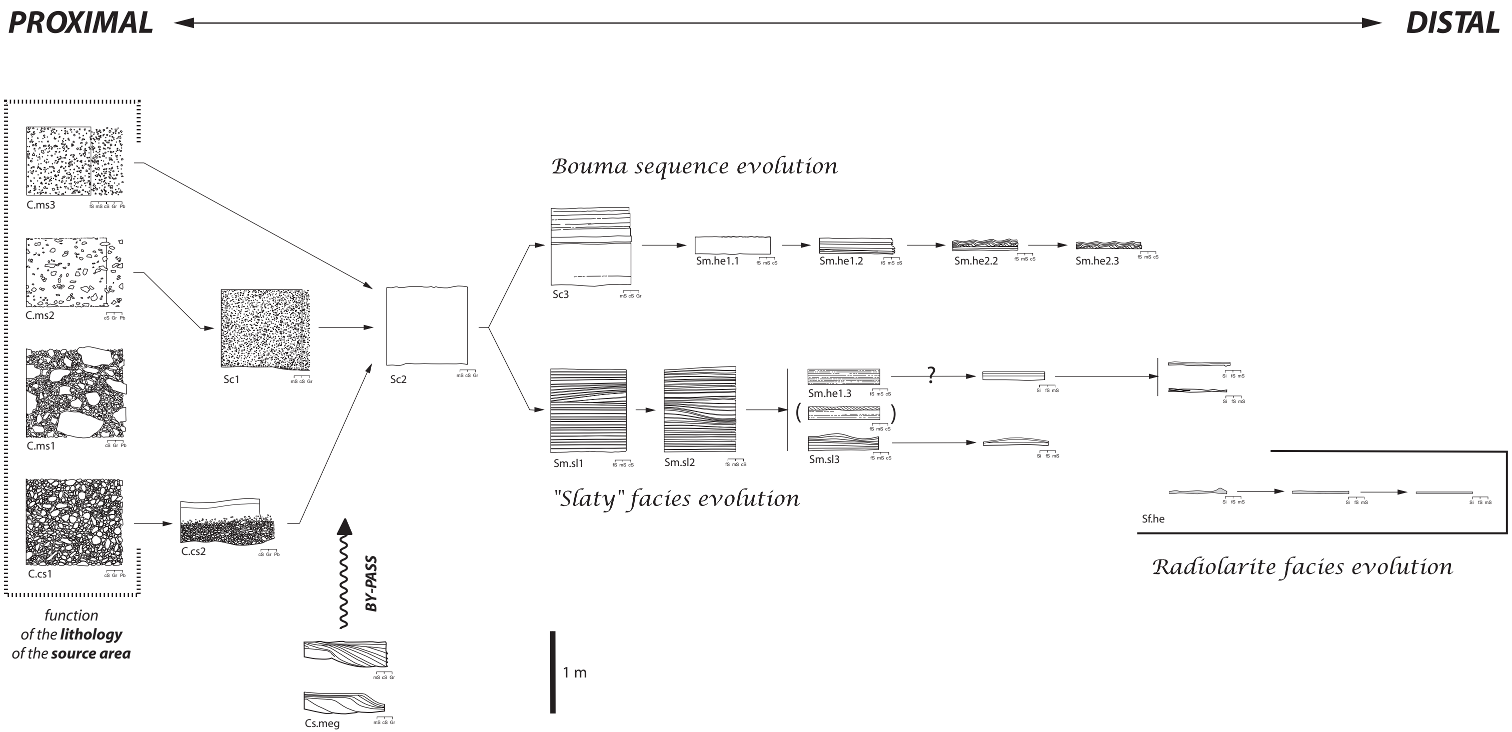


**Fig. 8.** Facies model: facies zonation and lateral substitution along a proximal–distal trend.

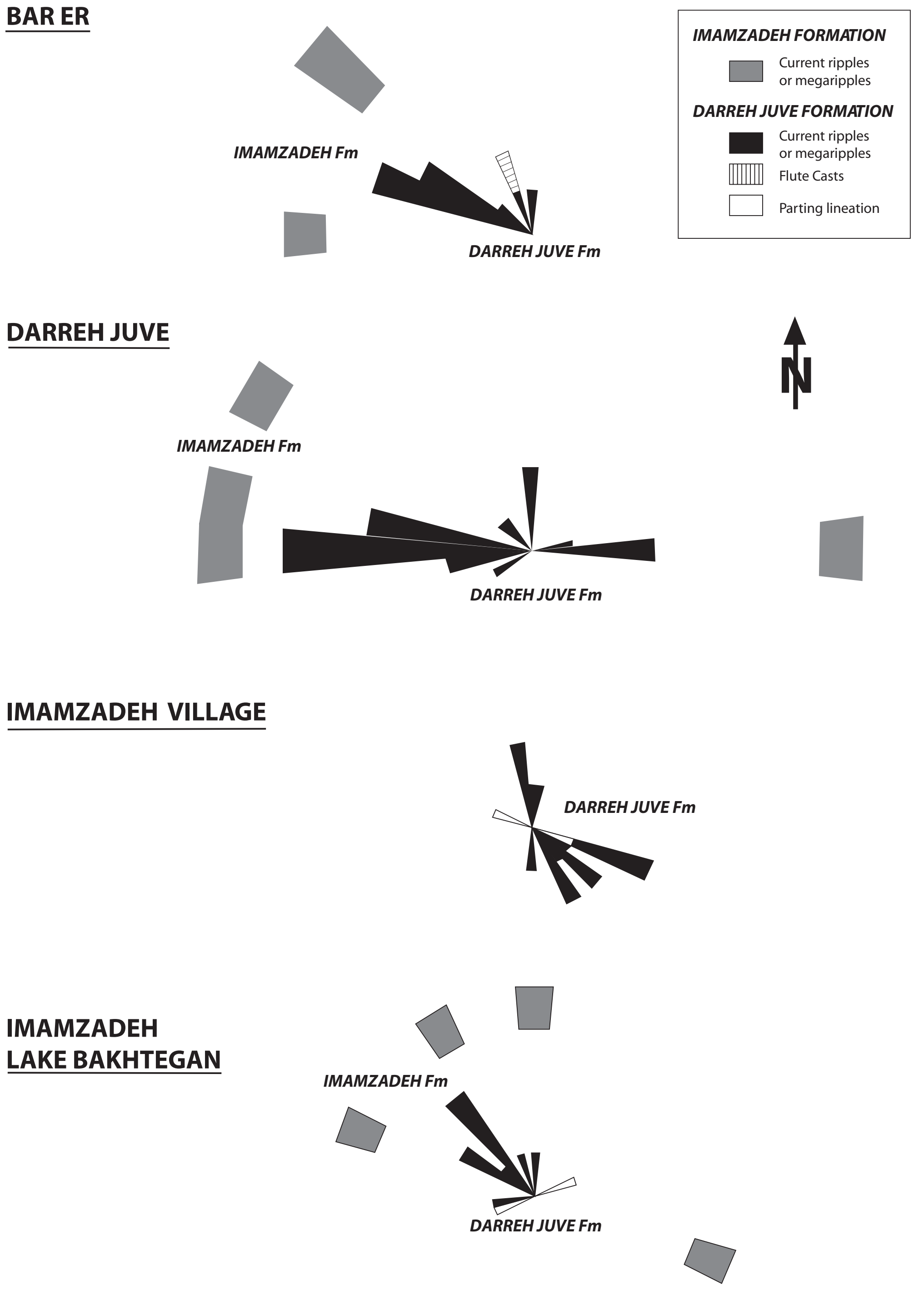


**Fig. 9.** Palaeocurrent measurements.

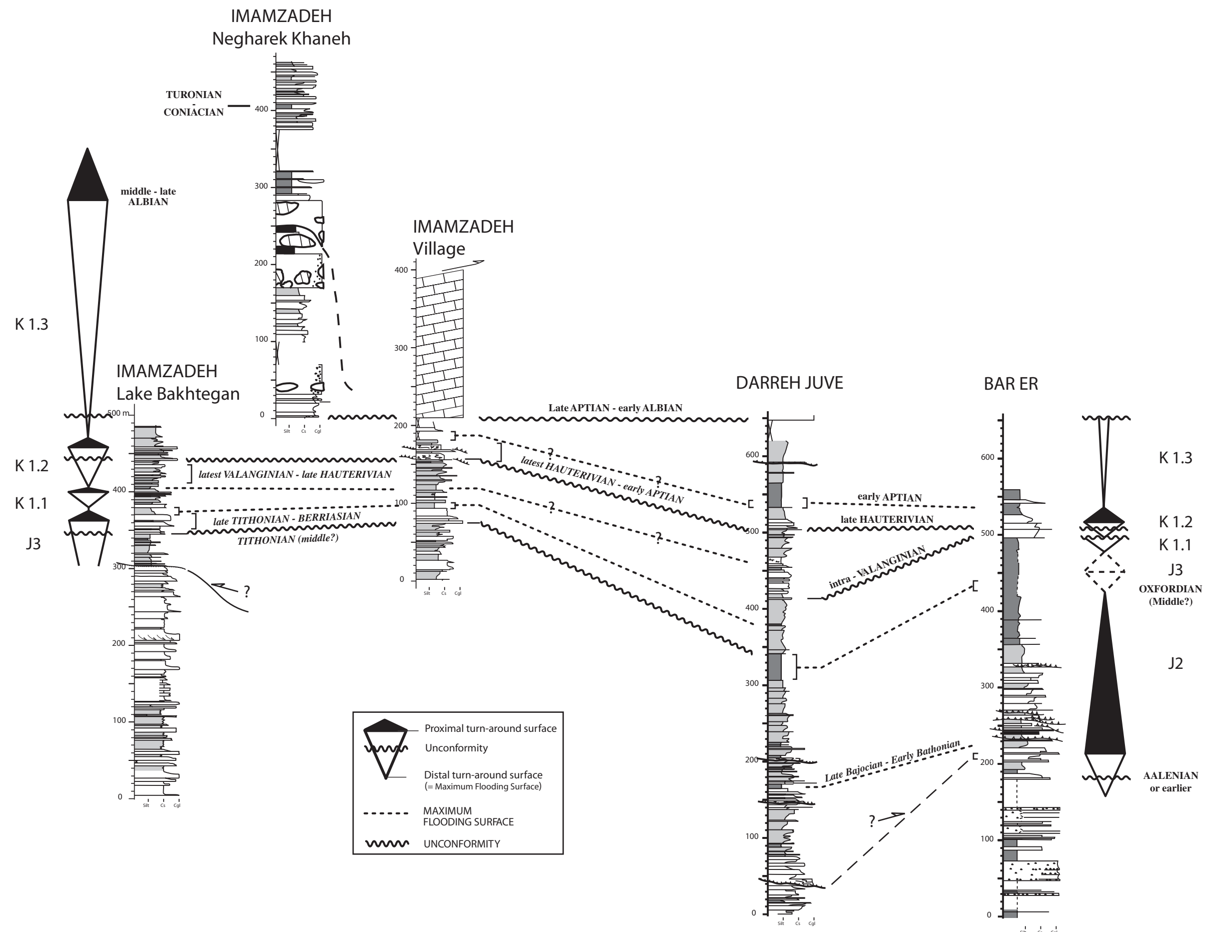


**Fig. 10.** Biostratigraphic and sequence stratigraphic correlations of the five studied sections: sequence definitions. The proximal turn-around surface corresponds to the occurrence of the most proximal facies along the depositional profile (Fig. 8). This surface either may coincide with the unconformity or may occur later. An *a priori* relationship with the flooding surface on the shelf is not expected.

correlations at this time scale. These third-order cycles are well recorded in the Darreh Juve Fm. At a higher time-scale duration (around 100 Ma), the two periods recording the most proximal facies (large debris flows, in this case) are the base of the Bar Er Fm (Triassic) and the base of the Neghareh-Khaneh Fm (latest Aptian to middle–late Albian).

Cycle J2 (Fig. 10) corresponds to the Darreh Juve Formation, which displays different stratigraphic patterns: the Imamzadeh–Lake Bakhtegan section is on one side and the Darreh Juve–Bar Er sections are on the other. In the Darreh Juve–Bar Er sections, cycle J2 is dominated by a distal-up trend. A sharp unconformity is recorded during the proximal-up trend. The age of the unconformity is poorly constrained: it occurred during the Aalenian or earlier. The proximal turn-around surface is Early Bajocian, possibly latest Aalenian. In the Imamzadeh–Lake Bakhtegan section, an aggradational to proximal-up trend is recorded. No age is available. The most proximal facies are recorded in Imamzadeh–Lake Bakhtegan (debris flows, hyperconcentrated to concentrated flows, with some low erosional channels: proximal lobe deposits) and the most distal one is in Bar Er (rare concentrated flows and by-pass deposits, numerous medium-density turbidity currents, some slumps: middle to distal lobes). In the Imamzadeh–Lake Bakhtegan section, a sharp erosional transition occurred at the top of the formation, directly overlain by medium- to low-density turbidity current deposits of middle to late Oxfordian age. This top erosional discontinuity could be a hiatus, a time-equivalent of the retrogradational trend recorded in the Darreh Juve–Bar Er sections.

The age constraint (i.e. the third-order maximum flooding surface of Late Bajocian–Early Bathonian age) between the Darreh Juve and the Bar Er sections indicate a pinching out of the sediments from Darreh Juve to Bar Er. It may record a truncation (onlap) of the base of the formation. This truncation suggests a tilting of this domain after the basal sharp unconformity of Aalenian age or earlier, characterized by intraformational conglomerates in the Bar Er section. The tilting can explain the occurrence of numerous *in situ* slumps in the middle to distal lobe deposits.

Third-order cycles (several tens of metres thick) are bounded by reddish to greenish claystones to siltstones. They probably record a break in the carbonate supply from the platform (i.e. a condensed interval and maximum flooding surface).

Cycle J3 (Fig. 10) corresponds to the base of the Imamzadeh Formation. Two stratigraphic patterns were recognized. In the Imamzadeh area, the cycle is very well recorded with a sharp unconformity (a downward shift of facies). In the Darreh Juve and Bar Er sections, the time-equivalent sediments have been identified only in biostratigraphic correlations. The unconformity is recorded only in the Darreh Juve section. The base maximum flooding surface (i.e. the most distal facies) overlaid sediments of middle Callovian to early Oxfordian age (i.e. the Darreh Juve Formation) and is capped by late Oxfordian to Kimmeridgian sediments (i.e. the Imamzadeh village sequence) and probably middle to late Oxfordian deposits (the age of the sediments overlying the hiatus of the Imamzadeh–Lake Bakhtegan section, which may contain the maximum flooding surface). An Oxfordian age, probably middle Oxfordian, can be proposed for this maximum flooding surface. The unconformity occurs approximately during the middle part of the Tithonian (Imamzadeh–Lake Bakhtegan).

Cycle K1.1 (Fig. 10) corresponds to the middle part of the Imamzadeh Formation. This cycle does not show a well-recorded unconformity, except in the Imamzadeh–Lake Bakhtegan section. This cycle is more condensed (less than 10 m thick) in the Bar Er section. It is stacked with an overlying sequence at the base of the upper member of the Imamzadeh Formation. The maximum time span of the entire cycle is late Tithonian to Valanginian; a more precise dating within this interval is not possible with radiolarian biostratigraphy. Based on the position within the cycle, the base maximum flooding surface is probably of Berriasianage. The unconformity probably occurred during Valanginian time. No age is available for the proximal turn-around surface.

Cycle K1.2 (Fig. 10) corresponds to the top of the Imamzadeh Formation. This cycle is characterized by a sharp downward shift of facies (unconformity) in all four sections where this cycle is exposed. No age is available for the maximum flooding surface at the base. The unconformity is bounded below by sediments of late Valanginian to Hauterivian age and just above by sediments of late Hauterivian to Barremian age. This suggests a Late Hauterivian age for this unconformity, with an error bar starting earlier in the Hauterivian and ending during the early Barremian. The proximal turn-around surface is of Barremian age.

Cycle K1.3 (Fig. 10) corresponds to the Neghareh Khaneh Formation. This cycle is characterized by a sharp unconformity. This is the most important downward shift of facies in all of the studied unconformities. The top maximum flooding surface is difficult to localize. Only one section (Imamzadeh–Neghareh Khaneh) shows this transition (Fig. 10). Unfortunately, this interval of around 50 m is badly exposed. Scarce outcrops of fine-grained sediments suggest distal environments for these deposits. The relationship with the overlying sediments (i.e. the top of the Neghareh

Khaneh Formation), which is mainly aggradational, is unknown.

The maximum flooding surface at the base is of early Aptian age (i.e. the Bar Er section). The unconformity is bounded below by early to middle Aptian age sediments and overlain by middle to late Albian sediments. A late Aptian to early Albian age is suggested for this unconformity. The proximal turn-around surface occurred during the middle to late Albian. No age is available for the maximum flooding surface at the top.

## Discussion: tectonic v. eustatic control of the stratigraphic cycles (Fig. 11)

The J2 cycle unconformity (Aalenian or earlier, Fig. 11) is the time-equivalent of a major tectonic unconformity of late Toarcian age (176 $\pm$ 2 Ma, GTS 2004), occurring at the Arabian platform scale (Sharland *et al.* 2001; the base of the AP7 tectonostratigraphic megasequence). Palaeogeographical changes (Ziegler 2001) suggest a reactivation of the more or less northward-trending Precambrian structures, dividing the Arabian plate into two domains: the Central Arabian Arch and the Ghawar–Safanyia fault system. Eastward of this axis (i.e. the present-day Arabian Gulf to Oman), the consequence of this deformation is a southward extension of the subsiding domain (i.e. the Dhruma Fm carbonate platform). The continental siliciclastic input sharply decreases.

This intraplate deformation event could have recorded the first stage of the continental rifting of the Somali Ocean, which is well known on its southern Madagascar margin (the Toarcian Morondova Basin, Geiger *et al.* 2004).

The J3 cycle maximum flooding surface (MSF; Oxfordian, probably middle Oxfordian, Fig. 11) occurred at the time of major marine flooding across the Arabian platform in the Jurassic period. This flooding event ranged from the Middle Callovian (MFS J40 of Sharland *et al.* 2001; Haq & Al-Qahtani 2005) to the Late Kimmeridgian (MFS J100, Sharland *et al.* 2001). Six minor flooding events have been defined (Sharland *et al.* 2001). The only one occurring in the Oxfordian is of Middle Oxfordian age (MFS J50, 158 Ma, GTS 2004). It corresponds to the most important MFS of the Late Jurassic (Haq & Al-Qahtani 2005); condensed organic-rich limestones of the Hanifa Fm).

This Late Jurassic (Middle Oxfordian to Kimmeridgian) flooding event occurred across the entire Arabian platform and East African domain (i.e. from southern Tanzania to western Ethiopia). It is limited to the Somali Ocean margin. It does not correspond to the major eustatic sea-level high event that occurred later (Tithonian, Haq *et al.* 1987).

The J3 cycle unconformity (Tithonian, probably middle Tithonian, Fig. 11) is also a time-equivalent to a major tectonic unconformity. It has been dated from the Early Tithonian (149.5 Ma, Gradstein 2004) by Sharland *et al.* (2001); the base of the AP8 tectonostratigraphic megasequence of Sharland. Again, palaeogeographical changes (Ziegler 2001) suggest a reactivation of the more or less northward-trending Precambrian structures (i.e. the Central Arabian Arch and Ghawar–Safanyia fault system), and of the NNE–SSW Dibba fault, bounding the present-day Oman Mountains westward. This unconformity records a long-wavelength tilting of the Arabian plate westward (Murris 1980) with superimposed reactivated Precambrian structures. In Oman, this tilting is coeval with a shoreline retreat of at least 200 km (Droste & van Steenwinkel 2004).

This unconformity probably records an intraplate deformation, related to the end of the Somali Ocean rift and the beginning of the oceanic accretion between Africa–Arabia on one side and Madagascar–India on the other (i.e. the first preserved magnetic anomaly on the oceanic crust: chron M22, the base Tithonian, Cochran 1988; Coffin & Rabinowitz 1988).

The K1.1 cycle maximum flooding surface (probably Berriasian, Fig. 11) on the platform could be the time-equivalent of the base Berriasian maximum flooding surface (MFS K10; marine shales from the Sulaiy Fm (Qatar and Abu Dhabi) and Rayda Fm (Oman), Sharland *et al.* 2001). According to Haq & Al-Qahtani, (2005), it corresponds to the major MFS of the cycle, ranging from the base Tithonian unconformity to the Late Valanginian unconformity.

The K1.1 cycle unconformity (Fig. 11), undated but ranging from the Berriasian to the base Hauterivian, could correspond either to the late Valanginian unconformity of Sharland *et al.* (2001) or to the Early Valanginian major eustatic fall of Haq *et al.* (1987). The relationship of Sharland's Late Valanginian unconformity with Haq's eustatic fall is unclear, but the major eustatic sea-level fall, of probable climatic origin, is clearly recorded on the Oman carbonate platform (Le Bec 2003).

The K1.2 cycle unconformity (late Hauterivian, Fig. 11) was not recognized by Sharland *et al.* (2001) or Haq & Al-Qahtani (2005) as a major unconformity on the Arabian platform. It does not correspond to any eustatic sea-level fall (Haq *et al.* 1987). The Hauterivian carbonate deposits of the Oman platform (Le Bec 2003) are tectonically controlled. This instability seems to be limited to the outer platform at the transition to the slope.

The K1.3 cycle maximum flooding surface (early Aptian, Fig. 11) on the platform could be

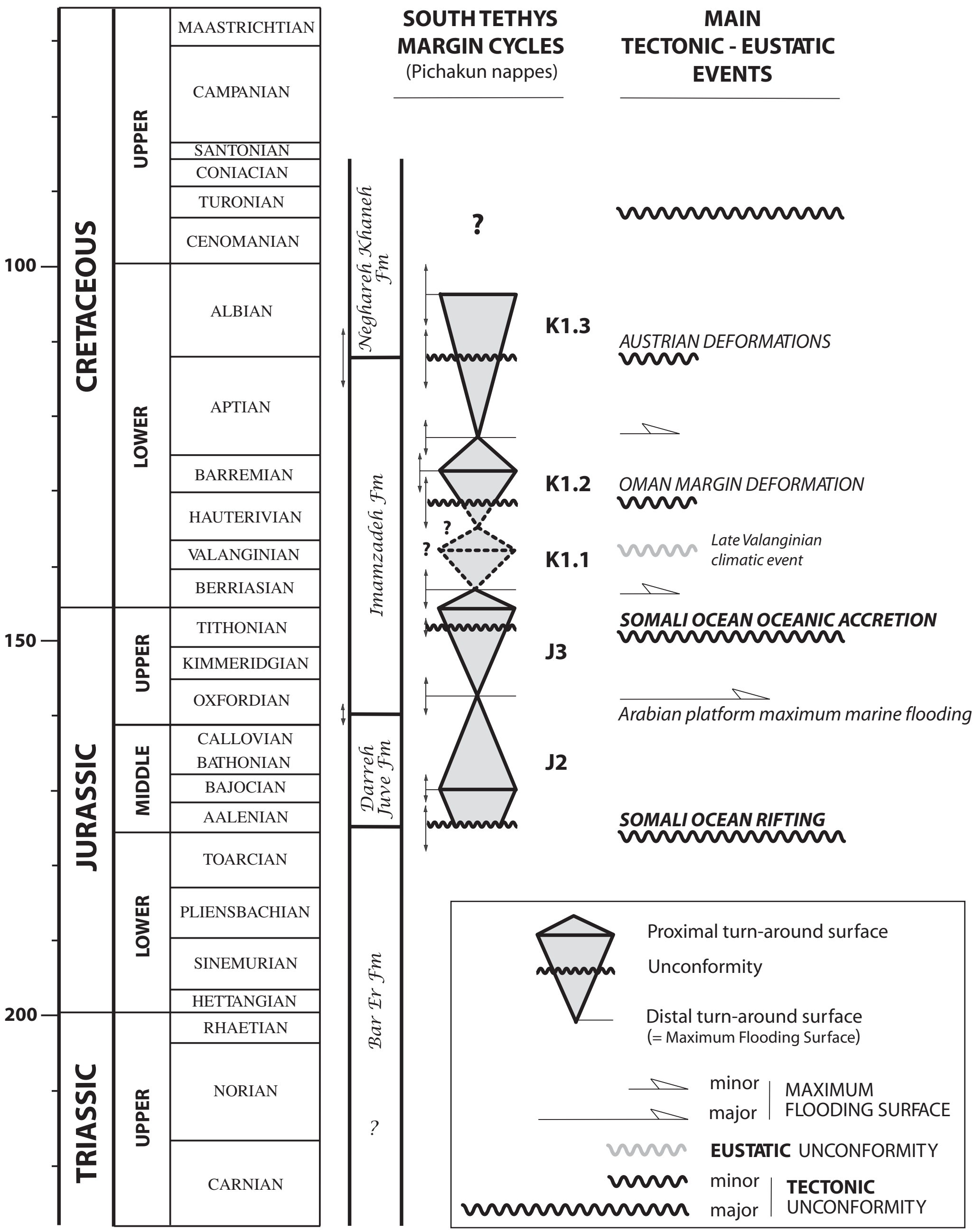


**Fig. 11.** Evolution of the southern Tethys margin based on the Pichakun Nappes data: biochronostratigraphy, sequence stratigraphy, tectonic and eustatic controls.

the time-equivalent of the base Aptian maximum flooding surface (K70, Sharland *et al.* 2001); that is, the base Shu'aiba Fm or the Hawar Fm. According to Haq & Al-Qahtani (2005), it corresponds to the major MFS of a cycle, ranging from the Late Valanginian unconformity to the Late Aptian unconformity.

This MFS is time-equivalent to a minor eustatic sea-level high (Haq *et al.* 1987), but records a major marine flooding along the southern margin of

Tethys and the African margin of the Somali and Mozambique oceans (Harris *et al.* 1984; Dercourt *et al.* 2000).

The K1.3 cycle unconformity (late Aptian–early Albian, Fig. 11) corresponds to a major tectonic unconformity (Harris *et al.* 1984; Christian 1997; Droste & van Steenwinkel 2004), dated as Late Aptian by Sharland *et al.* (2001). It corresponds to the boundary between the carbonate Dariyan Fm and the shaly Kazhdumi Fm (Iran, James & Wynd 1965) and between the Shu'aiba Fm and the Nahr Umr Fm (Bahrain to Oman, Droste & van Steenwinkel 2004). According to Sharland *et al.* (2001), this unconformity is not as important as the Late Toarcian and Early Tithonian ones. This tectonic unconformity is coeval with a widespread siliciclastic influx over the Arabian plate (clays to sands). This unconformity probably records the intraplate deformation related to the beginning of the convergence between Africa–Arabia and Eurasia (Austrian deformations *sensu lato*).

## Conclusion

Four main lithostratigraphic formations have been defined and dated in the Pichakun Nappes, an inversion of the southern Tethyan margin during the latest Cretaceous: (1) the Bar Er Formation (probably Late Triassic to Early Jurassic); (2) the Darreh Juve Formation (Aalenian–early Bajocian to middle Callovian–early Oxfordian); (3) the Imamzadeh Formation (middle Callovian–early Oxfordian to Aptian); (4) the Neghareh Khaneh Formation (late Aptian to Turonian–Coniacian).

Most of the sediments are deep-sea gravity-flow lobe deposits. Few channel deposits occur (i.e. the Darreh Juve Formation in the Imanzadeh–Lake Bakhtegan section). Some deeply incised channels (canyons?) were observed in the lower member of the Neghareh Khaneh Formation (Albian). Twenty-seven facies, grouped into eight facies associations, were defined. The texture of the proximal conglomeratic facies (i.e. clast-supported v. matrix-supported) is highly dependent of the nature (i.e. petrology, grain size) of the source area sediments. The boundary between debris flows and high-density turbidity currents is difficult to characterize in these conglomeratic facies. A specific facies association, in comparison with the 'classical' turbiditic facies model of Mutti (1992) (i.e. the 'slaty' facies), has been defined here. It corresponds to a stacking of planar to subplanar lamina-sets that are a few centimetres thick. Growing HCS-like structures can develop. In this study, radiolarians are reworked by low-density currents. Pelagic radiolarites were not encountered.

Two main palaeogeographical units have been characterized in the Pichakun nappes: proximal deep-sea deposits (i.e. nappes from the Imanzadeh area; lobes and channels) and distal ones (i.e. nappes from Bar Er and Darreh Juve; only lobes). Palaeocurrent measurements suggest a complex topographic pattern. The deposition occurred in a narrow deep-sea plain (a few hundred kilometres in size), located between the Arabian platform and seaward isolated carbonate platforms.

The most important discontinuity is located at the boundary between the Imamzadeh and Neghareh Khaneh Formations (i.e. the Aptian–Albian boundary, a deposit of olistoliths that are few metres to hundreds of metres thick in debris flows). Five second-order cycles (10–30 Ma duration), defined between two successive distal facies time-intervals, are proposed: (1) J2 (Toarcian?–middle Oxfordian, unconformity: Late Toarcian–Aalenian); (2) J3 (middle Oxfordian–Berriasian, unconformity: middle? Tithonian); (3) K1.1 (Berriasian–undated top); (4) K1.2 (undated base–early Aptian, unconformity: late Hauterivian); (5) K1.3 (early Aptian to at least Turonian–Coniacian, unconformity: Aptian–Albian boundary).

All of the main tectonic events recorded by the Arabian platform during this time interval (Sharland *et al.* 2001) have been identified as major unconformities in the Iran deep-sea record: the late Toarcian (plate deformation as a result of the beginning of the rifting of the Somali Ocean), early Tithonian (oceanic accretion in the Somali Ocean) and Aptian–Albian (Austrian deformations) events. In the study area, the most important event corresponds to the Aptian–Albian deformations. It is expected that another tectonic event occurred during the late Hauterivian. The late Valanginian eustatic fall, of climatic origin, seems to be recorded as an unconformity in the Iran southern Tethys margin sediments.

This study has been carried out and funded by the MEBE (Middle East Basins Evolution) programme, and was sponsored by AGIP-ENI, BP, the CNRS, Petronas, Shell, Total and UPMC. We thank E. Barrier and M. F. Brunet (CNRS-Université Pierre et Marie Curie, Paris 6), the managers of this programme and O. Saidi, the director of the Iran Geological Survey, for their help. A review by F. H. Nader (Institut Français du Pétrole) greatly improved the quality of the paper.

## References

ALAVI, M. 1994. Tectonics of the Zagros orogenic belt of Iran: new data and interpretations. *Tectonophysics*, **229**, 211–238.

AL-HUSSEINI, M. I. 1997. Jurassic sequence stratigraphy of the western and southern Arabian Gulf. *GeoArabia*, **2**, 361–382.

ALLEN, J. R. L. 1973. A classification of climbing-ripple cross-lamination. *Journal of the geological Society, London*, **129**, 537–541.

ALLEN, J. R. L. 1982. *Sedimentary Structures: their Character and Physical Basis*. Developments in Sedimentology, **30**, Elsevier, Amsterdam.

BAUMGARTNER, P. O., BARTOLINI, A. *ET AL*. 1995. Middle Jurassic to Early Cretaceous radiolarian biochronology of Tethys based on Unitary Associations. *In*: BAUMGARTNER, P. O., O'DOGHERTY, L., GORICAN, S., URQUHART, E., PILLEVUIT, A. & DE WEVER, P. (eds) *Middle Jurassic to Lower Cretaceous Radiolaria of Tethys: Occurrences, Systematics, Biochronology*. Mémoires de Géologie (Lausanne), **23**, 1013–1038.

BÉCHENNEC, F., LE MÉTOUR, J., RABU, D., BOURDILLON-DE-GRISSAC, C., DE WEVER, P., BEURRIER, M. & VILLEY, M. 1990. The Hawasina Nappes: stratigraphy, palaeogeography and structural evolution of a fragment of the south-Tethyan passive continental margin. *In*: ROBERTSON, A. H. F., SEARLE, M. P. & RIES, A. C. (eds) *The Geology and Tectonics of the Oman Region*. Geological Society, London, Special Publications, **49**, 213–223.

BERBERIAN, M. & KING, G. C. P. 1981. Towards a paleogeography and tectonic evolution of Iran. *Canadian Journal of Earth Sciences*, **18**, 210–265.

BERNOUILLI, D. & WEISSERT, D. 1987. The Upper Hawasina nappes in the central Oman mountains: stratigraphy, palinspastics and sequence of nappe emplacement. *Geodinamica Acta*, **1**, 47–58.

BLECHSCHMIDT, I., DUMITRICA, P., MATTER, A., KRYSTYN, L. & PETERS, T. 2004. Stratigraphic architecture of the northern Oman continental margin; Mesozoic Hamrat Duru Group, Hawasina Complex, Oman. *GeoArabia*, **9**, 81–132.

BOUMA, A. H. 1962. *Sedimentology of some Flysch Deposits: A Graphic Approach to Facies Interpretation*. Elsevier, Amsterdam.

BOURGEOIS, J. 1983. Hummocks – do they grow? *AAPG Bulletin*, **67**, 428.

BRAUD, J. 1989. *La suture du Zagros au niveau de Kermanshah (Kurdistan iranien): reconstitution paléogéographique, évolution géodynamique, magmatique et structurale*. Thèse d'Etat, Université de Paris-Sud (Paris XI).

CHRISTIAN, L. 1997. Cretaceous subsurface geology of the Middle East region. *GeoArabia*, **2**, 239–256.

COCHRAN, J. R. 1988. Somali Basin, Chain Ridge, and origin of the northern Somali Basin gravity and geoid low. *Journal of Geophysical Research*, **93**, 11985–12008.

COFFIN, M. F. & RABINOWITZ, P. D. 1988. Evolution of the conjugate East African–Madagascan margins and the western Somali Basin. Geological Society of America, Special Paper, **226**, 1–78.

DERCOURT, J., GAETANI, M. *ET AL*. 2000. *Peri-Tethys Atlas; Palaeogeographical Maps; Explanatory Notes*. Commission for the Geologic Map of the World, Paris.

DE WEVER, P., BOURDILLON-DE GRISSAC, C. & BEURRIER, M. 1988. Radiolaires sénoniens de la Nappe de Samail (Oman). *Revue de Micropaléontologie*, **31**, 166–179.

DROSTE, H. & VAN STEENWINKEL, M. 2004. Stratal geometries and patterns of platform carbonates: the Cretaceous of Oman. *In*: EBERLI, G. P., MASAFFERO, J. L. & SARG, J. F. R. (eds) *Seismic Imaging of Carbonate Reservoirs and Systems*. American Association of Petroleum Geologists, Memoirs, **81**, 185–206.

DUMITRICA, P. & DUMITRICA-JUD, J. 1995. *Aurisaturnalis carinatus* (Foreman), an example of phyletic gradualism among saturnalid-type radiolarians. *Revue de Micropaléontologie*, **38**, 195–216.

DUMITRICA, P. & DUMITRICA-JUD, R. 2005. *Hexasaturnalis nakasekoi* nov. sp., a Jurassic saturnalid radiolarian species frequently confounded with *Hexasaturnalis suboblongus* (Yao). *Revue de Micropaléontologie*, **48**, 159–168.

DUMITRICA, P., IMMENHAUSER, A. & DUMITRICA-JUD, R. 1997. Mesozoic radiolarian biostratigraphy from Masirah Ophiolite, Sultanate of Oman. Part I: Middle Triassic, uppermost Jurassic and Lower Cretaceous spumellarians and multisegmented nassellarians. *Bulletin of National Museum of Natural Science*, **9**, 1–106.

EBERLI, G. P. 1991. Calcareous turbidites and their relationship to sea-level fluctuations and tectonism. *In*: EINSELE, G., RICKEN, W. & SEILACHER, A. (eds) *Cycles and Events in Stratigraphy*. Springer, Berlin.

GEIGER, M., CLARK, D. N. & METTE, W. 2004. Reappraisal of the timing of the breakup of Gondwana based on sedimentological and seismic evidence from the Morondava Basin, Madagascar. *Journal of African Earth Sciences*, **38**, 363–381.

GORICAN, S. 1994. *Jurassic and Cretaceous radiolarian biostratigraphy and sedimentary evolution of the Budva Zone (Dinarides, Montenegro)*. Mémoires de Géologie (Lausanne), **18**, 176.

GORICAN, S., CARTER, E. S. *ET AL*. 2006. *Catalogue and systematics of Pliensbachian, Toarcian and Aalenian radiolarian genera and species*. Zalozba ZRC/ZRC Publishing, ZRC SAZU, Ljubljana.

GRABOWSKI, G. J., JR. & NORTON, I. O. 1994. Tectonic controls on the stratigraphic architecture and hydrocarbon systems of the Arabian Plate. *In*: AL-HUSSEINI, M. I. (ed.) *Geo'94. The Middle East Petroleum Geosciences, I*. GulfPetroLink, Bahrain, 413–436.

GRADSTEIN, F. M., OGG, J. G. & SMITH, A. G. (eds) 2004. *A Geological Time Scale*. Cambridge University Press, Cambridge.

HALLAM, A. 1976. Geology and plate tectonics interpretation of the sediments of the Mesozoic radiolarite–ophiolite complex in the Neyriz region, southern Iran. *Geological Society of America Bulletin*, **87**, 47–52.

HANDFORD, C. R. & LOUCKS, R. G. 1993. Carbonate depositional sequences and systems tracts—responses of carbonate platforms to relative sea-level changes. *In*: LOUCKS, B. & SARG, R. J. (eds) *Carbonate Sequence Stratigraphy: Recent Developments and Applications*. American Association of Petroleum Geologists, Memoirs, **57**, 3–41.

HAQ, B. U. & AL-QAHTANI, A. M. 2005. Phanerozoic cycles of sea-level change on the Arabian Platform. *GeoArabia*, **10**, 127–160.

HAQ, B. U., HARDENBOL, J. & VAIL, P. R. 1987. Chronology of fluctuating sea levels since the Triassic. *Science*, **235**, 1156–1167.

HARMS, J. C. 1975. Stratification and sequences in prograding shoreline deposits. *In*: HARMS, J. C., SOUTHARD, J. B., SPEARING, D. R. & WALKER, R. G. (eds) *Depositional Environments as Interpreted from Primary Sedimentary Structures and Stratification Sequences*. Society of Economic Paleontologists and Mineralogists, Short Courses, **2**, 81–102.

HARRIS, P. M., FROST, S. H., SEIGLIE, G. A. & SCHNEIDERMANN, N. 1984. Regional unconformities and depositional cycles, Cretaceous of the Arabian Peninsula. *In*: SCHLEE, J. S. (ed.) *Interregional Unconformities and Hydrocarbon Accumulation*. American Association of Petroleum Geologists, Memoirs, **36**, 67–80.

HOMEWOOD, P. W., MAURAIAUD, P. & LAFONT, F. 1999. *Best practices in sequence stratigraphy for explorationists and reservoir engineers*. Centre de Recherche Elf Exploration–Production, Mémoire, **25** [in French].

JAMES, G. A. & WYND, J. G. 1965. Stratigraphic nomenclature of Iranian oil consortium agreement area. *AAPG Bulletin*, **49**, 2182–2245.

JUD, R. 1994. *Biochronology and Systematics of Early Cretaceous Radiolaria of the Western Tethys*. Mémoires de Géologie (Lausanne), **19**, 147.

KNELLER, B., EDWARDS, D., MCCAFFREY, W. & MOORE, R. 1991. Oblique reflection of turbidity currents. *Geology*, **14**, 250–252.

LAPIERRE, H., SAMPER, A. *ET AL*. 2004. The Tethyan plume: geochemical diversity of Middle Permian basalts from the Oman rifted margin. *Lithos*, **74**, 167–198.

LE BEC, A. 2003. *Distribution et dynamique des systèmes carbonatés de la plate-forme crétacé inférieur du Sultanat d'Oman*. Thèse de Doctorat, Université Michel de Montaigne (Bordeaux 3), Bordeaux.

LE MÉTOUR, J., MICHEL, J. C., BÉCHENNEC, F., PLATEL, J. P. & ROGER, J. 1995. *Geology and mineral wealth of the Sultanate of Oman*. MPM Geological Documents. Directorate General of Minerals, Ministry of Petroleum and Minerals, Sultanate of Oman, Muscat.

LE NINDRE, Y. M., MANIVIT, J., MANIVIT, H. & VASLET, D. 1990. Stratigraphie séquentielle du Jurassique et du Crétacé en Arabie Saoudite. *Bulletin de la Société Géologique de France*, **VI**, 1025–1034.

MURRIS, R. J. 1980. Middle East: Stratigraphic evolution and oil habitat. *AAPG Bulletin*, **64**, 597–618.

MUTTI, E. 1979. Turbidites et cônes sous-marins profonds. *In*: HOMEWOOD, P. (ed.) *Sédimentation détritique (fluviatile, littorale et marine).* Institut de Géologie, Université de Fribourg, Fribourg, 353–419.

MUTTI, E. 1985. Turbidite systems and their relations to depositional sequences. *In*: ZUFFA, G. G. (ed.) *Provenance of Arenites*. NATO Advanced Studies Institutes Series. Serie C: Mathematical and Physical Sciences, 148. D. Reidel Publishing, Dordrecht, 65–93.

MUTTI, E. 1992. *Turbidite Sandstones*. Agip, Milan.

MUTTI, E., TINTERRI, R., REMACHA, E., MAVILLA, N., ANGELLA, S. & FAVA, L. 1999. An introduction to the analysis of ancient turbidite basins from an outcrop perspective. *American Association of Petroleum Geologists, Continuing Education Course Note Series*, **39**, 96.

O'DOGHERTY, L. 1994. *Biochronology and Paleontology of Mid-Cretaceous Radiolarians from Northern Apennines (Italy) and Betic Cordillera (Spain).* Mémoires de Géologie (Lausanne), **21**, 413.

O'DOGHERTY, L. & GUEX, J. 2002. Rates and pattern of evolution among Cretaceous radiolarians: relation with global paleoceanographic events. *Micropaleontology*, **48**, Supplement 1, 1–22.

PHILIP, J. 2003. Peri-Tethyan neritic carbonate areas: distribution through time and driving factors. *Palaeogeography, Palaeoclimatology, Palaeoecology*, **196**, 19–37.

PICKERING, K. T. & HISCOTT, R. N. 1985. Contained (reflected) turbidity currents from the Middle Ordovician Cloridorme Formation, Quebec, Canada: an alternative to the antidune hypothesis. *Sedimentology*, **32**, 373–394.

PILLEVUIT, A., MARCOUX, J., STAMPFLI, G. & BAUD, A. 1997. The Oman Exotics: a key to the understanding of the Neotethyan geodynamic evolution. *Geodinamica Acta*, **10**, 209–238.

POMAR, L. 2001. Types of carbonate platforms: a genetic approach. *Basin Research*, **13**, 313–334.

POSAMENTIER, H. W., JERVEY, M. T. & VAIL, P. R. 1988. Eustatic controls on clastic deposition I—Conceptual framework. *In*: WILGUS, C. K., HASTINGS, B. S., KENDALL, C. G. S. C., POSAMENTIER, H., ROSS, C. A. & VAN WAGONER, J. (eds) *Sea-level Changes: an Integrated Approach*. Society of Economic Paleontologists and Mineralogists, Special Publications, **42**, 109–124.

RICOU, L. E. 1976. *Evolution structurale des Zagrides: la région-clé de Neyriz (Zagros iranien)*. Mémoire de la Société Géologique de France, Nouvelle Série, **125**, 140.

SANFILIPPO, A. & RIEDEL, W. R. 1985. Cetaceous Radiolaria. *In*: BOLLI, H. M., SAUNDERS, J. B. & PERCH-NIELSEN, K. (eds) *Plankton Stratigraphy*. Cambridge University Press, Cambridge, 573–630.

SCHLAGER, W., REIJMER, J. J. G. & DROXLER, A. 1994. Highstand shedding of carbonate platforms. *Journal of Sedimentary Petrology*, **B64**, 270–281.

SEARLE, M. P. & GRAHAM, G. M. 1982. 'Oman exotics': oceanic carbonate build-ups associated with the early stages of continental rifting. *Geology*, **10**, 43–49.

SHANMUGAM, G. 1996. High-density turbidity currents: are they sandy debris flows? *Journal of Sedimentary Research*, **66**, 2–10.

SHANMUGAM, G. 2000. 50 years of the turbidite paradigm (1950s–1990s): deep-water processes and facies models—a critical perspective. *Marine and Petroleum Geology*, **17**, 285–342.

SHARLAND, P. R., ARCHER, R. *ET AL*. 2001. *Arabian Plate Sequences Stratigraphy*. GeoArabia, Special Publication, **2**, 371.

STAMPFLI, G., MARCOUX, J. & BAUD, A. 1991. Tethys margins in space and time. *Palaeogeography, Palaeoclimatology, Palaeoecology*, **87**, 373–409.

STOCKLIN, J. 1968. Structural history and tectonics of Iran—a review. *AAPG Bulletin*, **52**, 1229–1258.

Van Wagoner, J. C., Posamentier, H. W., Mitchum, R. M., Vail, P. R., Sarg, J. F., Loutit, T. S. & Hardenbol, J. 1988. An overview of the fundamentals of sequence stratigraphy and key definitions. *In*: Wilgus, C. K., Hastings, B. S., Kendall, C. G. S. C., Posamentier, H., Ross, C. A. & Van Wagoner, J. (eds) *Sea-level Changes: an Integrated Approach*. Society of Economic Paleontologists and Mineralogists, Special Publications, **42**, 39–45.

Van Wagoner, J. C., Mitchum, R. M. J., Campion, K. M. & Rahmanian, V. D. 1990. *Siliciclastic sequence stratigraphy in well logs, cores, and outcrops: concepts for high resolution correlation of time and facies*. American Association of Petroleum Geologists, Methods in Exploration Series, **7**, 55.

Ziegler, M. 2001. Late Permian to Holocene paleofacies evolution of the Arabian Plate and its hydrocarbon occurences. *GeoArabia*, **6**, 445–504.